Politecnico di Torino

Master's Degree in Automotive Engineering – Product Development
A.y. 2024/2025
Graduation Session March 2025

Design and development of a non-return valve for cooling systems of automotive applications

Supervisor:
Prof. Massimo Rundo

Candidate:
Andrea Fachino

Company Supervisors:
Ing. Jean Baptiste Bedrignans
Ing. Gabriele Ranocchia

Summary

The aim of this stage activity and thesis work, done in collaboration with "*RAICAM DRIVELINE srl*", is the design and development of a non-return valve for cooling systems of Automotive applications.
This work follows a series of subsequent steps, starting from a preliminary research and benchmarking activity to characterize the technical specifications and characteristics of existing unidirectional valves. Afterwards these outcomes will be used for the proper valve design, including 3D modeling through Computer Aided Design (CAD) software, component development and sizing to respect all the imposed requirements and working conditions. A key step will be the material selection for the case study to ensure the feasibility of the assembly processes.
This preliminary valve sizing will be checked through Computational Fluid Dynamics (CFD) simulation, mainly to analyze the pressure drops across it.
Once the valve has been designed a first functional prototype will be manufactured and subsequently tested following a Concept Validation plan defined for this specific application.
Finally, these experimental results will be used for the tuning of CFD valve model in order to get a reliable model for future development in other similar applications.

Acknowledgements

Prima di iniziare la discussione di questa tesi, vorrei esprimere la mia più profonda gratitudine a tutte le persone che, con il loro supporto, hanno reso possibile il raggiungimento di questo importante traguardo.

Innanzitutto vorrei ringraziare il mio relatore, il Prof. Massimo Rundo, per l'interessamento e la collaborazione durante l'intera durata del progetto ma anche la disponibilità nella scrittura di questa tesi

Ringrazio Raicam per la possibilità di svolgere il mio lavoro di tesi presso la loro azienda, per i software e apparecchiature messe a disposizione e per il tempo dedicato alla mia formazione.
In particolare ringrazio il tutor aziendale ed il team con cui ho avuto piacere di collaborare per la riuscita di questo progetto, Jean Baptiste, Gabriele e Matteo.
Un ringraziamento va anche ai colleghi d'ufficio presso Raicam per l'accoglienza, gli insegnamenti e la collaborazione ricevuti durante il periodo di tirocinio in azienda.

Un grazie speciale va alla mia famiglia per il supporto e la possibilità di intraprendere questo percorso di studi, sostenendomi in ogni momento e lasciandomi sempre libero di fare le mie scelte.

E last but not least, un grazie a tutti i miei amici, in particolare ai Fellas, per esserci sempre stati durante questi anni di università, per i periodi di svago e divertimento passati in compagnia.
Grazie ai coinquilini di casa Gioberti, per i momenti trascorsi assieme a Torino e non, ai compagni conosciuti durante i corsi in magistrale al Poli.

Table of Contents

List of Tables

List of Figures

1 Introduction

This project is linked to the growing importance on the market of electrification and hybridization of vehicles, which is leading toward the continuous development of electric motors with increasing range, larger capacity of battery systems and increasing complexity of electric systems.
This causes the need to have an increase in complexity and improved layout of the cooling system to dissipate the heat produced by all these electric components and guarantee extended lifespan of EV motors.
Thus, the cooling system is needed to maintain the components in its respective working temperature for a favorable performance and high efficiency, so it needs to be designed to efficiently cool, or in some cases of low temperature and cold start conditions to heat, all the components for optimum performances.
To make this possible the cooling system is usually composed of many different loops, with various size, length and complexity to reach all the parts to cool down, all connected to the main radiator of the vehicle.
A simple scheme of an electric vehicle cooling system is here reported in figure 1.1. [1]

Figure 1-1: Example of cooling system layout for an electric vehicle

The main loops of the cooling systems may be interconnected by using different types of valves [2], such as multi-way valves (figure 1.2a), diverters and pipes (figure 1.2b). The first are used to split or combine coolant flows and to route the media inside the pipelines, the latter have the main task to collect the flow between radiators and different elements of the cooling system, resisting in all possible working conditions.

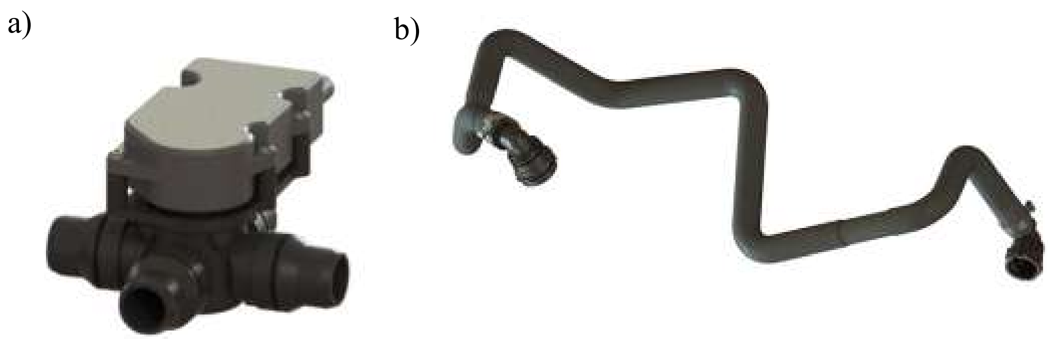

Figure 1-2: Example of: a) multiway valve and b) pipes for a cooling system

When the flow of liquid coolant must follow a unidirectional path a specific kind of valve is used, the *non-return valve*, also called unidirectional valve or check-valve in jargon. This device, depicted in figure 1.3, is employed to avoid the backflow of the liquid inside the circuit, represented by the cooling system, against the direction of the fluid stream imposed by the pump. This function is important for many reasons: it helps in reducing the coolant pump's dimension and energy consumption, but still avoiding malfunctioning of the system for a higher reliability. Furthermore, this device is designed to guarantee a good sealing action when the valve is closed while low pressure losses in the positive flow direction through the cooling system, allowing to maintain an optimal pressure levels within the cooling system.
These kinds of products were already widely developed and adopted for ICEs cooling applications but they are returning to be the subject of studies for continuous improvement to satisfy some new requirements for the latest kind of applications for advanced thermal management strategies.

Figure 1-3: Example of unidirectional valve CAD model

1.1 Product general characteristics

The main needed features for this kind of product are all linked to its area of use, therefore to electrified vehicles.
In general, a vehicle's cooling system must be able to cope with a variety of different situations and temperature conditions, so that it can adjust as needed the flow of liquid through its plumbing system.
In particular the main objectives are those of having a low volume, reduced weight and dimensions object to reduce the overall mass and footprint of the cooling system which usually contains more than a single valve, at least one for each of its loops, to guarantee a correct uniform and unidirectional flow in all the pipes.
Furthermore, it has to be a simple product to reduce the complexity, cost and installation issues related to each of these components but still ensure high reliability in a wide range of working conditions.

Lastly, this kind of product has to be produced in large volume to reduce its unitary cost, making the standardization of the process to obtain it and the concept of modularity very important, hence using the same body of the valve for multiple layouts and applications.

All these aspects will be considered in the next steps to try to develop a competitive product, with the final aim to avoid buying it from external suppliers while starting a future manufacturing and assembly process inside the company.

1.2 Functional specifications

In addition to the general features described in the above section, the main technical constraints and specifications of the product are imposed by the customer's requirements, in this case study application by the *Group PSA*, whose entire layout is here reported in figure 1.4.

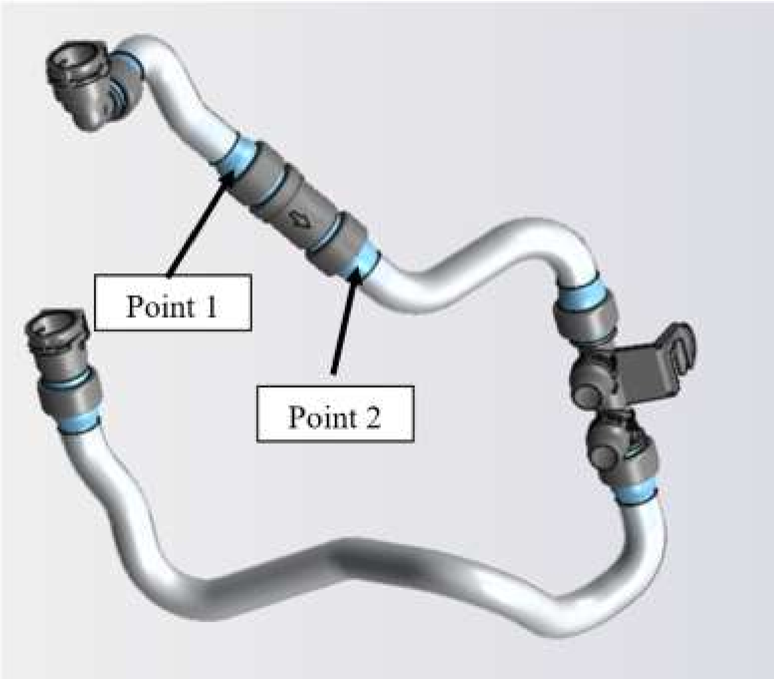

Figure 1-4: CAD assembly of cooling system

The client imposes the parameters required and the working conditions for our product, which is a non-return valve specific for the Low Temperature Loop of the vehicle's cooling system, in which the flow direction is specified and reported in the previous model (Figure 1-4) from point 1 to point 2.

Overall the system is composed of the following main elements, each identified by the corresponding letter in figure 1.5:

A. One double-T connector with the mounting support to attach it to the vehicle structure according to its designed configuration;

B. 4 pressure rings to ensure watertight connections and good sealing between the connectors and the pipes;

C. 1 unidirectional check valve (Figure 1-6 below);

D. 3 hoses, flexible and curved tubes to convey the coolant liquid inside the system.

E. 2 protection sleeves with a curved shape to provide a protective shield to the two longer and more curved hoses of the system.

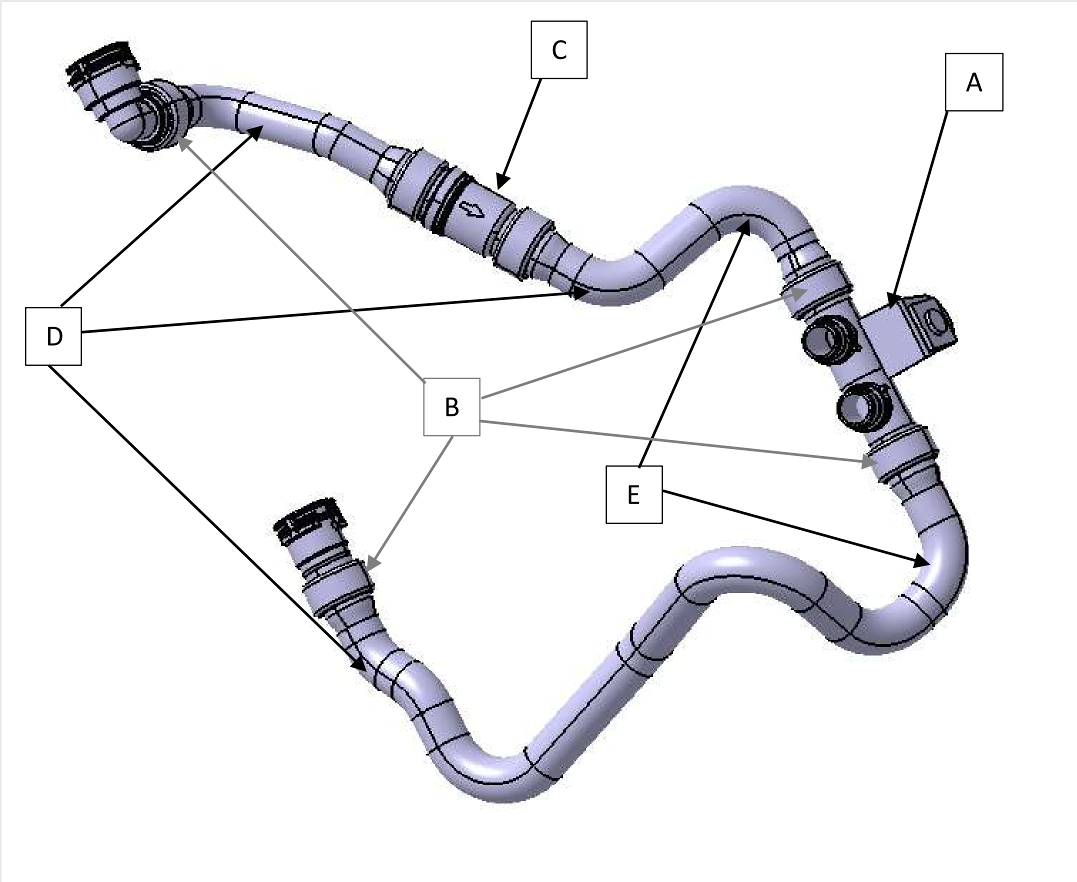

Figure 1-5: HK0 STEP2 LT LOOP - inlet battery charger pipe

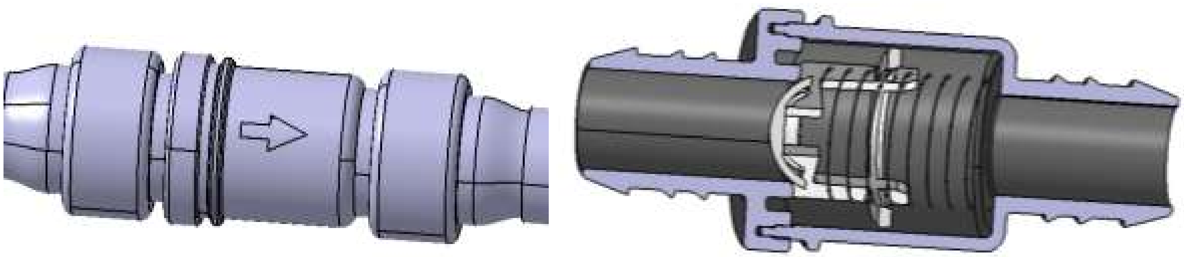

Figure 1-6: Detail on CAD unidirectional valve of the system

As it's possible to notice from the Figure 1-6 above, the single direction of the flow inside the valve is the one indicated by the arrow on the valve body; this is a key aspect to show the correct mounting direction of the component along the system pipes.
According to the standard, a quick connector (figure 1.5-A) is a device, consisting of a female and a male part, for establishing a fluid-tight connection between two pipes or between a pipe and a component/user without using other fastening elements and without need for maintenance.

Tests on the coupling elements are performed in an environment with controlled temperature, pressure and humidity; the main tests include:
- low temperature (-30 °C) and high temperature (90 °C);
- bursting pressure (max 6 bar);
- resistance to different chemical agents;
- static and dynamic mechanical tests.

In addition, *Raicam* requirements provide general design directives for specifying installation dimensions of fittings and hoses (figure 1.5-D) used on the vehicle's cooling systems, but also additional design constraints for parts which interact in coupling between a flexible connecting member (hose) and a rigid element (radiator, water pump, heater, etc.).
This assembly standardization between valve and other components has the aim to guarantee sealing under normal service conditions, while respecting dimensional accuracy and surface roughness tolerances, following some standard procedures.

The **coolant** used in this specific cooling system is a 50/50 mix of water and glycol, whose characteristics such as pressure (*p*), density (ρ), kinematic viscosity (*ν)* are reported in the table1.1 at the working temperature (*T*) of 60°C.

The kinematic viscosity of the liquid is defined as the dynamic (absolute) viscosity μ
of a liquid divided by its density at the same temperature. The viscosity of the fluid is strictly dependent of the temperature, in facts the higher the temperature the lower the viscosity.

Equation 1

$$\boldsymbol{\nu} = \frac{\mu}{\rho} \quad \left[\frac{m^2}{s}\right]$$

T [°C]	60
$p\ [mbar]$	1000
$\boldsymbol{\rho}\ \left[\frac{kg}{m^3}\right]$	1037.9
$\boldsymbol{\nu}\ \left[\frac{m^2}{s}\right]$	$13.3 * 10^7$
$\boldsymbol{\mu}\ [Pa * s]$	$1.38 * 10^{-3}$

Table 1.1: Liquid coolant properties

Many important aspects have to be considered when designing a valve. The primary ones are reported and explained in the following section [3].

The **pressure drop** across the unidirectional valve, also called pressure loss or delta-pressure, is calculated as the difference between the upstream (Point 1) and the downstream (Point 2) pressures of the valve represented in Figure 1-4, for each operating condition in terms of coolant temperature and volumetric flow rate.

Equation 2

$$\Delta p = p1 - p2\ [mbar]$$

The pressure loss between these two points, must respect the values reported below in table 1.2, imposed by the customer's requirements for this specific application whit the working fluid at 60 °C of temperature.

Pressure Drop (1→2)	
Q $\left[\frac{l}{min}\right]$	**Δp** $[mbar]$
5	3
10	6
15	10

Table 1.2: Pressure drops limit values

The maximum allowed pressure drop is reported as function of the volumetric flow rate; indeed, the valve must ensure a flux that can reach values up to 15 l/min during the most severe working conditions of the cooling system when the heat to dissipate is higher.
For that reason, the valve design including the opening width allowed by the spring and the section geometry, has to consider this requirement related to the maximum coolant volumetric flow to be guaranteed. The flow rate is typically specified at a point above the cracking pressure when the spring gets compressed and the valve is open, allowing the fluid stream through it.

Pressure loss is mainly caused by the frictional resistance of the walls, changes in the magnitude or direction of the fluid velocity or the valve's spring itself, but also other variables related to the liquid coolant used, such as fluid density, velocity, flow area and viscosity.
Thus, it is important to achieve a higher efficiency of the system since it will require a lower pumping work to drive the fluid inside the cooling system, consequently resulting in a lower dimension of the pumps, lower energy consumption and losses in the system.

Experimental tests on the physical valve to measure volumetric flow rate and the corresponding pressure loss have been performed during the benchmarking activity; all the details and explanations will be given in the next chapter of this thesis work (Chapter 2).

The **bypass flow**, also called internal leakage, is defined as the maximum flux of coolant allowed in direction opposite to the valve's imposed one to protect the equipment and system from over-pressure.
Its values are imposed at specific differential pressure levels between the extremes of the valve, for this specific application the maximum allowable bypass rate is 0.5 l / min with a differential pressure of 450 mbar and coolant temperature 60 °C.

The **cracking pressure** is defined as the minimum inlet pressure level required for a check valve to open [4]. This situation occurs when the fluid exerts a force on the valve that exceeds the force of the closing spring, deforming the spring inside the valve body and starting the stream.

In general, the cracking pressure is the lowest differential pressure that the valve experiences during the coolant stream and for this kind of application it’s stays in the range of the millibars.
Finally, the **bursting pressure** (or burst pressure) is the pressure at which the valve can survive without rupturing or bursting.
The burst pressure is usually defined among the critical characteristics of the valve, since it is the maximum pressure that can be applied to it without causing physical damage or destruction of the part.
According to the standard, this parameter must be tested at minimum 9 bar pressure at 90°C cooling liquid temperature, repeating 3 tests of 10 s duration each, with a rate of increase in pressure of at least 1 bar/s.
This procedure represents very severe testing conditions with respect to normal use conditions, both in terms of pressure level and pressure gradient; this is necessary to guarantee a high safety margin.

In the end some specific precautions have to be considered for the operation of the by-pass valve, it is required to remain the same regardless of its position in relation to the Earth's gravity, so that the cooling system and the valve works in the same way both at sea level and at higher altitudes.
Also consider the position and direction of assembly of the valve along the cooling system, which could be horizontal, vertical or oblique but must work properly in all the possible configurations of piping, making them suitable for any kind of installation with the right spring selection and geometry design.

2 Specifications identifications and Benchmarking analysis

Starting from the available data, technical drawings and requirements provided by the customers and suppliers the first goal is to identify the most important parameters and concepts before starting the design of our own product.

First of all, some technical drawings are provided; they will be useful to have a comprehensive and general idea about the physical dimensions and volumes of the product, so as to estimate the overall size of the part inside the system.
Some precise indications and data could be missing or hidden by the supplier for company's internal or confidential reasons.

Dimensions and surface requirements specified by the technical drawings:
Dimensional tolerances ±0.1 to ±0.5 [mm]
Surface roughness R_z=16 microns [μm] on the inlet and outlet mating surfaces of the valve external connections: where R_z measures the difference between the highest peak and lowest valley within the sampling length of five lines.

In addition, some physical copies of the product are given by two different suppliers: they will be analyzed and studied to compare their performance by carrying out some bench tests to quantify the characteristics of the valve physically available.
For confidential reasons the competitors' name will not be mentioned in this thesis work; their products under study will be called *valve #1* and *valve #2*.

Figure 2-1: Physical check valves under testing

The appropriate equipment and the methodology for evaluating differential characteristics and performances of the given check valves are depicted in this chapter.

The experimental tests explained in this section were carried out in person by availing the equipment and machinery present at "*RAICAM DRIVELINE srl*" plant.

2.1 Benchmarking: pressure drop

Testbench **equipment** (pictured in Figure 2-2 below):

A. Liquid tank with controlled temperature through electrical resistance to impose coolant temperature according to the functional specification requirements.
B. Pump to circulate working fluid and impose the volumetric flow rate from selector: according to the characterization of the system Q is linearly proportional to pump's power scale (adimensional value displayed on the controller). The technical details of the appliance are provided in the Appendix chapter A1.
C. Cooling system rubber pipes, made of *EPDM* (ethylene propylene diene monomer): 1 inlet to valve from liquid tank, 1 outlet of valve back to tank.
D. Connectors between pipes, tank and valve with metal ties for leakproof connections also at increasing pressure levels.
E. Temperature sensors to carry out test at the specification temperature (60 °C) and monitor eventual temperature gradient in the circuit.
F. Pressure sensors to measure pressure values at valve's inlet and outlet.

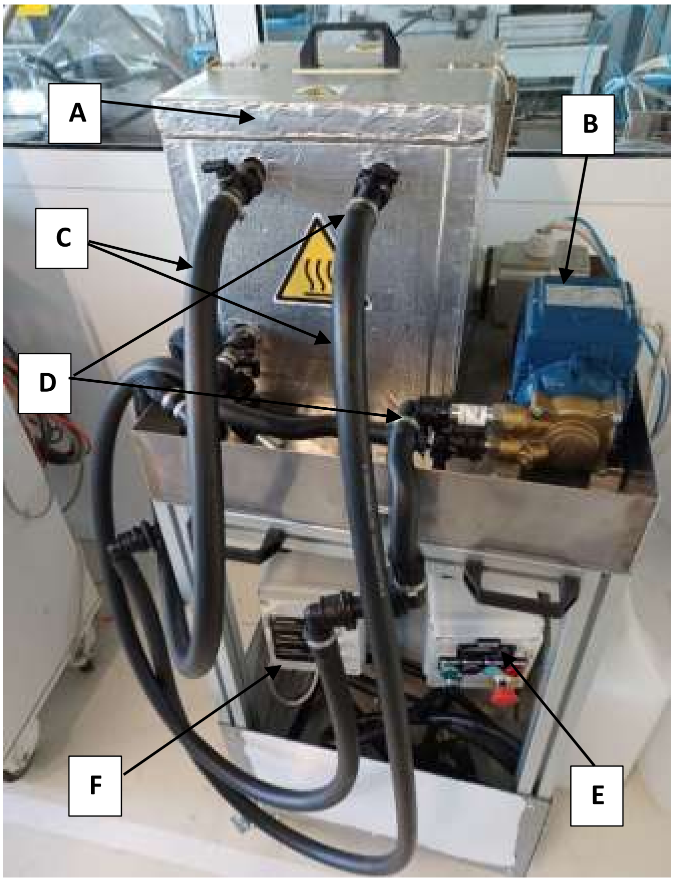

Figure 2-2: Testbench equipment

Important notice: the pressure sensors have a minimum sensitivity of 0.01 bar, which is one order of magnitude higher than the one needed to measure the pressure drops required, that are in the order of the *mbar*, therefore an alternative method of measurement will be discussed here.
At the same time the pipes and connectors mounted for the tests have a certain length, as depicted in figure 2.3, therefore not negligible pressure loss across them must be considered as well.
In addiction possible precision errors may arise during the tests and measurements.

Figure 2-3: Valve and pipes setup

According to the requirement the temperature must be controlled to have a 60°C flux through the valve; to achieve this it's necessary to impose a higher temperature to the thermocouple in the water box to consider heat losses in the circuit and obtain the target temperature, that is measured through a temperature sensor after the valve outlet.

Methodology:

- Variable pipes length according to application, consider worst case scenario with pump located at maximum distance from the pump to simulate maximum losses in the circuit and lower pressure level through the valve.

- Mount water column to measure difference in liquid height, between inlet and outlet of the valve, and obtain the correspondent difference in pressure in a very precise way. The setup used for the test is reported in Figure 2-4 .
  This is possible knowing the correlation between the water column height and ambient pressure (*p*).

  $$1\ \text{atm} = 10\ \text{m}_{h\text{-}H2O}$$

  This relationship can be demonstrated with the following calculations:

  Equation 3 $$p = \rho * g * h$$

  In which the water density ρ is approximated to 10^3 kg/m^3 and the acceleration of gravity *g* to 10 m/s^2, finally multiplying by the height *h* of the water column considered (10 m) the following pressure value at the bottom of the column is obtained:

  $p = 10^5$ N/m^2 = 10^5 Pa = 10 bar

  Therefore, knowing the conversion of the pressure unit *(1 atm = 1.013 bar)* and considering the height range of the water columns (*cm*) the relationship can be expressed as:

  Equation 4 $$\Delta h = \Delta p \rightarrow 1\text{cm}_{h\_H2O} = 1\ \text{mbar}$$

  Where $\Delta h = h1 - h2$ [mm] is the difference between inlet and outlet liquid columns, representing the minimum value that can be discretized and measured on the physical water columns.

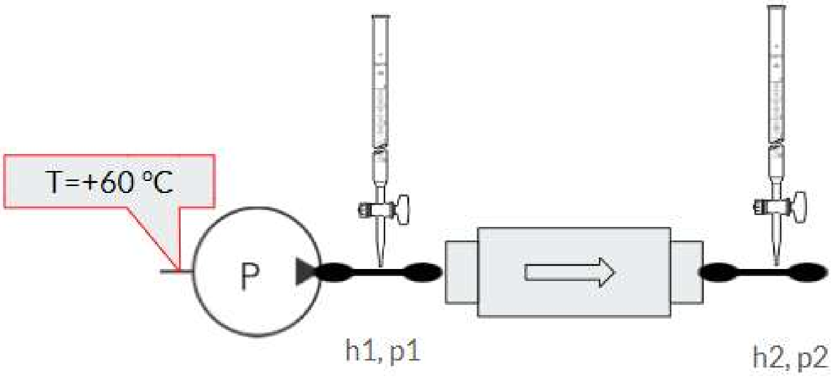

Figure 2-4: Scheme of p-drop test layout

- Measure difference in water columns heights to obtain related Δp, according to eq. (3), for the three prescribed values of volumetric flow rate (Q = 5 ,10 and 15 l/min) and all the intermediate steps, in particular at the lowest values to better discretize the working points around which the valve opens and the outlet pressure level starts changing.

Figure 2-5: Pressure drop test setup

- At each step of flow increase wait until steady state conditions are reached, so that the fluid stream through the valve is stable and the corresponding liquid column heights are fixed and can be measured.
- Compare measured pressure drops across the valve with the imposed limit ones (
- Table 1.2) for each flow rate configuration.

These heights of liquid column are obtained therefore only using very low-pressure levels in the open circuit, in the order of tens of millibars, meaning that the physical length of this test equipment will limit the measured flowrate values.

Data analysis valve #1:

The experimental measurements of difference in height and relative delta-pressure for each value of Q are here reported in Table 2.1.
A limitation of this experimental test was the height of the water columns, reason why the flow rate and delta-pressure measurements were stopped at a certain level (below 15 l/min) since higher values would have caused higher pressures, resulting in water escape above of the water column.

Pump scale [-]	Q [l/min]	Δh [cm]	Δp [mbar]
0	0		
0,1	0,33		
0,2	0,66		
0,3	0,99		
0,4	1,32		
0,45	1,48	9,4	9,4
0,5	1,65	11,6	11,6
0,6	1,97	15,2	15,2
0,7	2,30	17,4	17,4
0,8	2,63	18	18
0,9	2,96	18,3	18,3
1	3,29	18,6	18,6
1,46	**5**	20,7	20,7
1,5	5,01	21,1	21,1
2	6,58	23,5	23,5
2,5	8,23	25,8	25,8
2,94	**10**	27,6	27,6
3	10,10	28,3	28,3
3,5	11,52	29,8	29,8
3,68	12,11	30,8	30,8

Table 2.1: Pressure drop benchmarking results (#1)

As it's possible to notice in the previous table of experimental results, the first values of delta for Q below 1.4 l/min are not present since it's not meaningful to calculate delta pressure until the flux through the valve is null, with pressure values lower than the cracking one (around 9 mbar) and the outlet column height is constant.
These data were also plotted in Figure 2-6 to better analyze the trends of the pressure drop as a function of the volumetric flow rate through the valve:

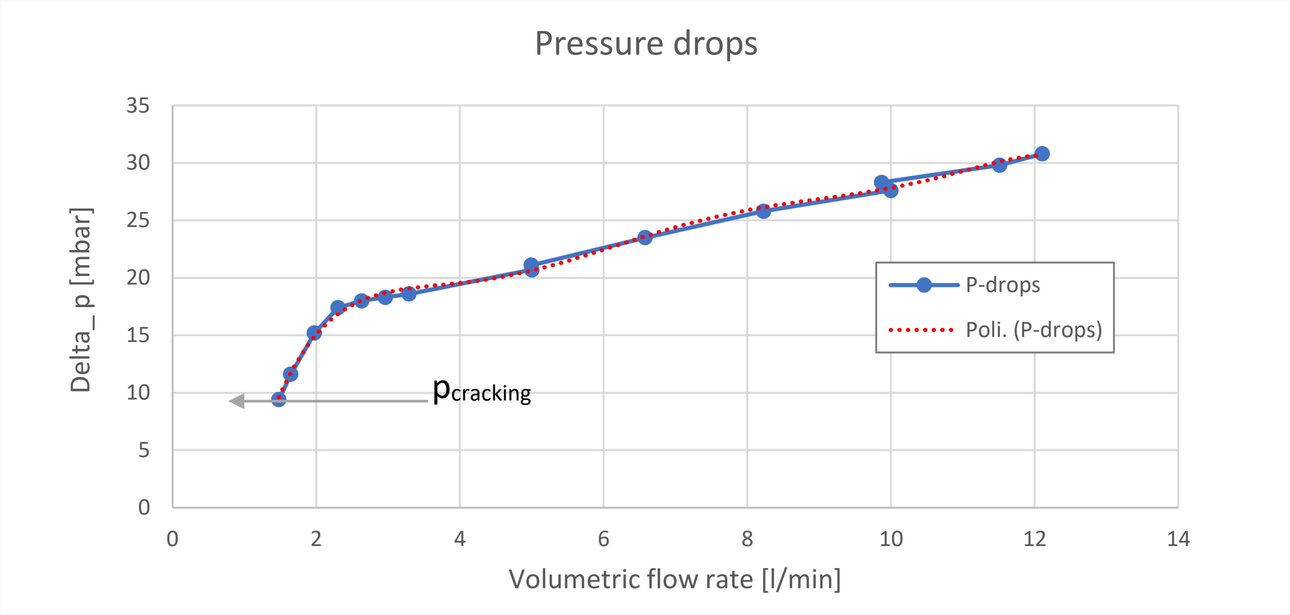

Figure 2-6: Pressure drop as function of flow rate

These experimental results seem to follow a polynomial approximation, highlighted on the plot by the dotted line, in particular when the volumetric flow rate Q is higher than 3 l/min the valve is already open ($p > p_{cracking}$) and the flow area increases with the displacement of the piston; in this part of the plot the results are just affected by valve's geometry and stream areas design.

Instead at low values of flow the valve is still closed by the spring force on the plunger, resulting in not linear and steep initial increase pressure drops caused by the starting null or reduced stream. For this part of the plot an higher spring rate results in higher slope.
In this range the observed height of the outlet column was constant, meaning that the outlet pressure value is still constant and not affected by upstream values.

The previous test was repeated using 2 pressure sensors, placed at inlet and outlet of connectors of the valve, instead of the water columns to overcome the problem of the limited flow rate measurable.
In this way it was possible to test the valve up to a flow of 30 l/min and calculating the pressure loss through it as the difference between the inlet and outlet sensor readings. Considering the sensitivity error of the sensors (± 10 mbar) the Δp was plotted accordingly in Figure 2-7 with the two lines representing the range of error:

- Δp_{Max} (red line) calculated from equation 2 with $p1_{Max}$ and $p2_{min}$.
- Δp_{min} (green line) calculated from equation 2 with $p1_{min}$ and $p2_{Max}$.

The main outcomes of this benchmarking activity were the results of the pressure drops values that are evidently not respecting the technical requirements imposed (

Table 1.2) but turned out being in line with the performances of other similar check valves by different competitors.

In facts the manufacturer of the valve tested declared much larger values of delta-pressure, reported in Table 2.2, with respect to the one showed above in Table 2.1, to be conservative and have a large safety margin in possible tests or checks by the client.

Q [l/min]	Δp [mbar]
9.3	69
11.4	100
12.4	120
15.7	207
19.8	345

Table 2.2: Competitor #1 declared pressure drops

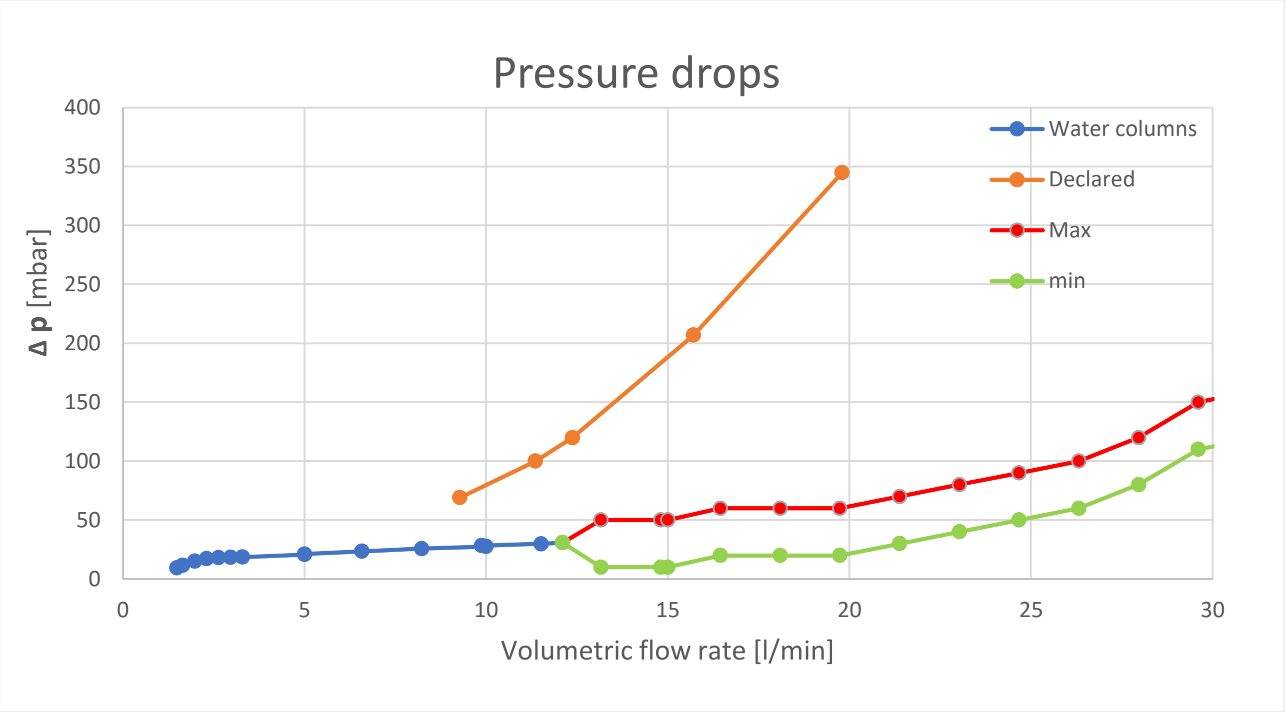

Figure 2-7: Pressure drops as function of flow rate

Data analysis valve #2:

This second valve tested showed very low experimental delta-pressure values, reported in table 6, very close to the ones imposed by the specification (Table 1.2).

As a consequence, it was possible to use the water columns measurements for all the volumetric flow rate values up to 15 l/min, in facts lower pressure levels resulted in lower liquid height below the physical limit dimensions.

Q [l/min]	Δp [mbar]
5	4.8
10	5.4
15	10.8

Table 2.3: Pressure drop results

The experimental results of this valve #2 was compared with the previously tested one, resulting in significant lower values, as evidenced in the following plot of Figure 2-8:

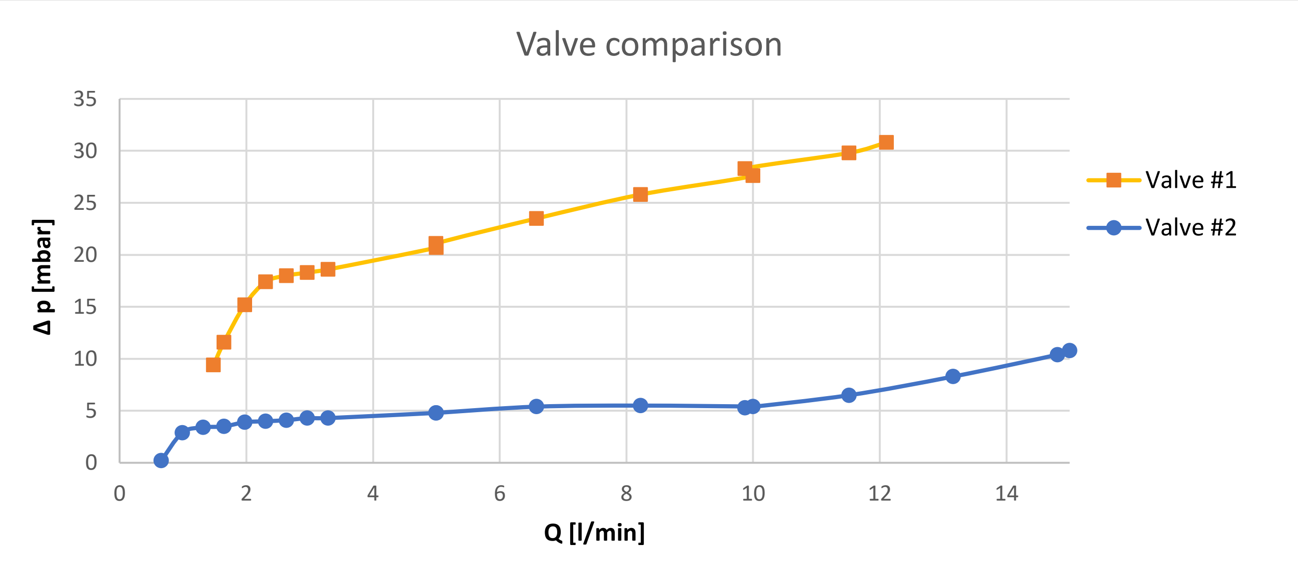

Figure 2-8: Pressure drop comparisons

In facts this lower pressure loss through this second valve is mainly influenced by its design: the larger internal flow area, the internal geometry to avoid abrupt stream restriction or change of direction and by very low spring stiffness that causes the valve to open quickly, reducing the pressure accumulated at its inlet ($p1$).

These factors and geometry will be considered for the future valve design in the next chapter of this thesis work.

2.2 Benchmarking: volumetric flow rate Q

The physical valves from both the external suppliers have been bench-tested to verify that they respect the target related to the volumetric flow rate, to allow Q values of 5 -10 -15 l/min.

Equipment (Open circuit test illustrated in Figure 2-9):

- Water pump and connecting pipes
- Graduated container to collect water at valve output.

Methodology:

- Increase power of pump upstream of valve, the volume flow rate increases linearly with pump power (linear characteristic reported in the Appendix…)
- Reach target flow rate value, Q_{target}, imposed through the valve for a certain testing time t (ex. 30, 20 and 10 s for increasing values of rate)
- Meanwhile collect and measure volume V of liquid at valve output, considering the limited volume (5 l) of the container.
- Compute average flow across valve as:

Equation 5

$$Q_{avg} = \frac{V}{t} \; \left[\frac{l}{min}\right]$$

- Compare Q_{target} and Q_{avg} and evaluate possible flow reduction through the valve in each operating condition.

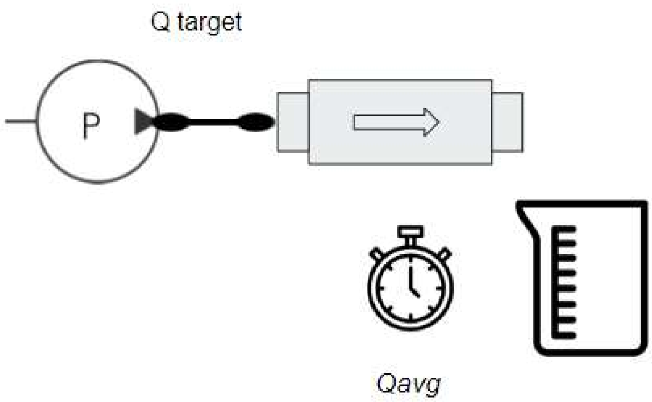

Figure 2-9: Scheme of volumetric flow rate test layout

Data analysis:
The main outcomes of this test on the valve #1 are summarized in the following Table 2.4.

Q_{target} [l/min]	Time [s]	Volume [L]	Q_{avg} [l/min]	Flow reduction [%]
5	30	2.35	4.7	6
10	20	3.25	9.75	2.5
15	10	2.45	14.7	2

Table 2.4: Volumetric flow rate experimental results valve #1

The results show that for increasing value of flow rate, resulting in more pressure and force to open the valve's spring, the flow reduction decreases to very low and therefore acceptable values, since there are no functional guidelines regarding these quantities. This stream reduction could be due to the fact that a part of the flow rate is used to create pressure inside the valve and keep it open acting against the spring preload.

The second valve tested (#2) shows a much larger stream area, much lower spring stiffness and preload, resulting in lower or null flux reduction through the valve. The experimental results are here reported in Table 2.5.

Q_{target} [l/min]	Time [s]	Volume [L]	Q_{avg} [l/min]	Flow reduction [%]
5	30	2.5	5	0
10	20	3.31	9.93	0.7
15	10	2.5	15	0

Table 2.5: Volumetric flow rate experimental results valve #2

2.3 Benchmarking: bypass flow

Equipment:

- Water pump with controlled temperature (60 °C according to specifications).
- Pressure sensor upstream valve exit, which is mounted in reverse direction to the liquid flow for this specific test, as schematized in Figure 2-10.
- Pc equipped with software "*banco misure funzionali comandi idraulici*" to display pressure values in real time. Figure 2-11

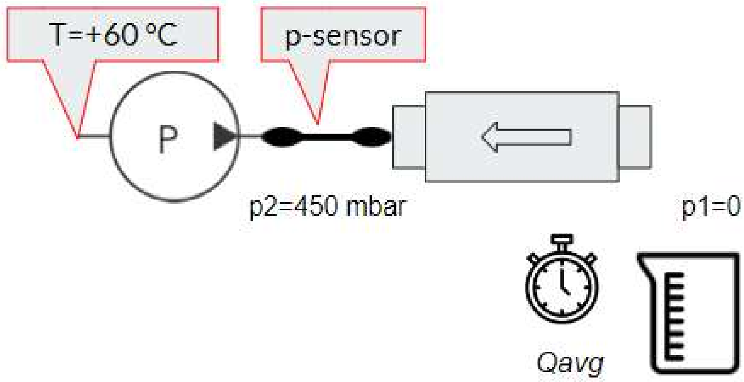

Figure 2-10: Scheme of bypass flow test layout

Figure 2-11: Pressure measurement and backflow test

Methodology:

- Impose $p2$ = 450 mbar at valve outlet (downstream the pump output), while leaving the pump inlet open $p1$ = 0, since the sensor measures the relative pressure with respect to the atmospheric value, to carry out a test with the delta-pressure imposed by the specification.
- Collect volume V of liquid at valve inlet during t test duration.
- Compute average flow across valve in time $Q_{avg}=V/t$ [l/min]
- Compare with the maximum allowed by specification in given working conditions.

Important notice: The bypass flow is not directly proportional to the pump pressure upstream of the valve output; in facts if *p2* increases, the higher backflow force on the plunger causes the valve closure by extending the spring and pushing the piston ball on its seat, resulting in a lower bypass.

Data analysis valve #*1*:

The outcomes of this specific test showed negligible values of bypass flow, less than 1 ml per minute of internal leakage for such a low value of pressure drop imposed by the requirement ($\Delta p = 450\ \mathrm{mbar}$)
The valve under test showed a good sealing action in all normal operating conditions, also increasing p-drop above 3 bar but still resulting in negligible internal leakages, even if the increase in pressure caused a slight deformation of the pipes but not backflow, as it was depicted in Figure 2-11.
The solution applied to prevent the bypass flow was the addiction of some material or rubber sealing elements to avoid leakages or the use of a rubber ball as a closing element, also called stopper or plunger, to enter in contact with the valve's seat; beyond this advantage, this solution has as drawback the additional cost of materials or increased complexity in the design and assembly phases.
These considerations will be important for the next design steps of the project.

Data analysis valve #*2*:

The other valve was tested in the same prescribed operating conditions, showing some bypass flow in the opposite direction of the valve's one, as pictured in Figure 2-12Figure 2-12
The internal leakage fluid was collected for one-minute of time, a volume *V* of 237 ml, obtaining the following average bypass flow:

$Q_{avg}=V/t = 0.237$ l/min

This value respected the bypass flow limit prescribed by specification for those testing conditions (0.5 l/min), thus also this second valve resulted being compliant even if not equipped of rubber sealing elements, resulting in lower complexity and material cost of the product.

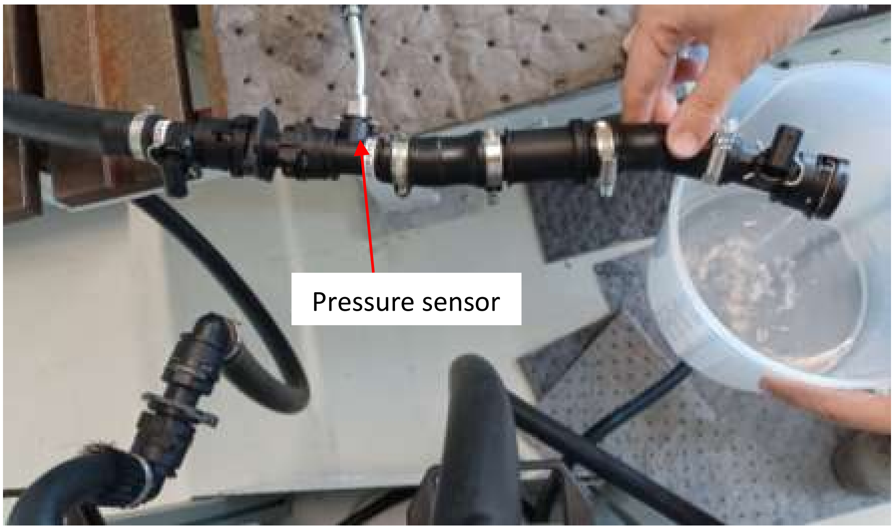

Figure 2-12: Bypass flow measurement

2.4 Valve's spring stiffness evaluation

- Spring material: stainless steel (AISI).
- Material mechanical properties:

  Modulus of Elasticity E = 193 GPa
  Poisson's Ratio v = 0.29
  Shear modulus G = 77 GPa

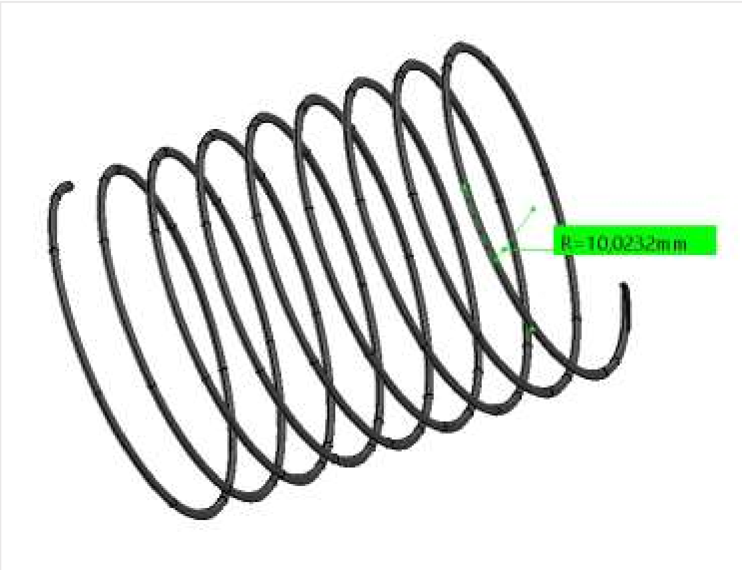

Figure 2-13: Example of spring CAD

- Quotes and information from CAD model of the spring:

  Number of active coils n = 8;
  Coil internal diameter d = 0.5 mm;
  Coil mean diameter D = 19 mm.

Knowing the material properties and given the spring geometry and dimensions, measured directly from the CAD model, it's possible to calculate the spring stiffness by using the following equation:

Equation 6

$$k = \frac{G\,d^4}{8\,D^3 n} \quad \left[\frac{N}{m}\right]$$

Using the available data and the right dimensional units of measure:

$$k = 10.96\ \mathrm{N/m} = 0.011\ \mathrm{N/mm}$$

This theoretical value will be compared with the one coming from the experimental test on a similar physical valve spring provided by a different manufacturer.

2.5 Benchmarking: spring stiffness experimental characterization

Equipment:

- Load cell “*Mark10*” with max capacity 100 N, minimum resolution 0.05 N. All system's technical information is reported in Figure 2-14- b.
- “Adapter arm” to transmit load between cell and stopper above the spring.
- Centering vice to align precisely the loading cell and spring center.

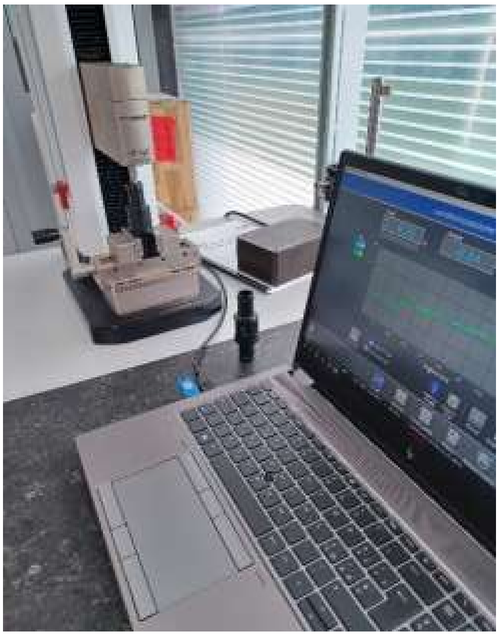

System Information:
IntelliMESUR Version: 2.1.3
Test Frame Model: F505
Test Frame Serial Number: 4374594
Test Frame Capacity: 500 lbF / 2.2 kN
Test Frame Firmware Version: 1.00.14
Force Sensor Model: FS05-20
Force Sensor Capacity: 100 N
Force Sensor Resolution: 0.05 N
Force Sensor Serial Number: 4384631
Calibration Date: Nov 18, 2023
Calibration Due Date: Nov 18, 2024

Figure 2-14: (a) Loading cell “Mark10” and (b) system information

- Control software “*IntelliMESUR*®” on PC, connected to the loading cell to set all the parameters for the test, monitor the results during the execution and export them afterwards [5].

Figure 2-15: Software IntelliMESUR®

Testing procedure:

- Set the lift [mm], load [N] and moving speed [mm/s] of the test.
  For the test case were used displacements comparable with the spring maximum one, directly measured with a digital comparator and rounded to 10 mm, by applying a load of 0.2 N with a low testing speed, around 30 mm/min to obtain slow and precise strokes.
- Set the home initial reference position for the measurements, identified by the position of contact between load cell and top of the piston.
- Select the maximum load or displacement of the up and down strokes, the test stops when one of those limits to protect the cell from overload.
- Start the cycle with an offset-distance above the contact with the valve spring, for example 1 mm, to allow the complete extension of the spring.
- Contact starts, then the spring deformation continues for the imposed stroke distance (usually less than 10 mm).
- Repeat the load-unload cycles more times, 4 cycles in the studied case, to be aware of possible cyclical variations.

Figure 2-16: Spring testing with loadcell

More tests were performed with different load and displacement configurations and only the most meaningful results were considered to show some acceptable experimental results.
Afterwards the spring stiffness was calculated as the ratio between the applied force F [N] and spring resulting displacement x [mm] from the initial configuration.

Equation 7

$$k = \frac{F}{x} \quad \left[\frac{N}{m}\right]$$

Data analysis for valve *#2*:

Important notice: some precision problems may arise since the minimum resolution of the instrumentation (0.05 N) is very close to the load to apply on the spring to deform it, as evidenced in Figure 2-17 in the force-displacement plot of the spring, that results in some step variations of the measured load by the cell because of its sensitivity.

Also consider not negligible inertia of "adaptor arm" between cell and spring during the repeated up/down strokes that could slightly influence the measurements.

A meaningful characterization was obtained with F = 0.2 N and x = 10 mm, resulting in an estimate spring stiffness of 0.020 N/mm, which highlights the extremely low stiffness of this second tested spring. This will be a key parameter for the valve design and performances, since it's strictly linked to the valve cranking and by-pass pressures.

This slope (red line in the figure) was obtained through an extension test therefore the force decreases with the displacement of the spring during the elongation.

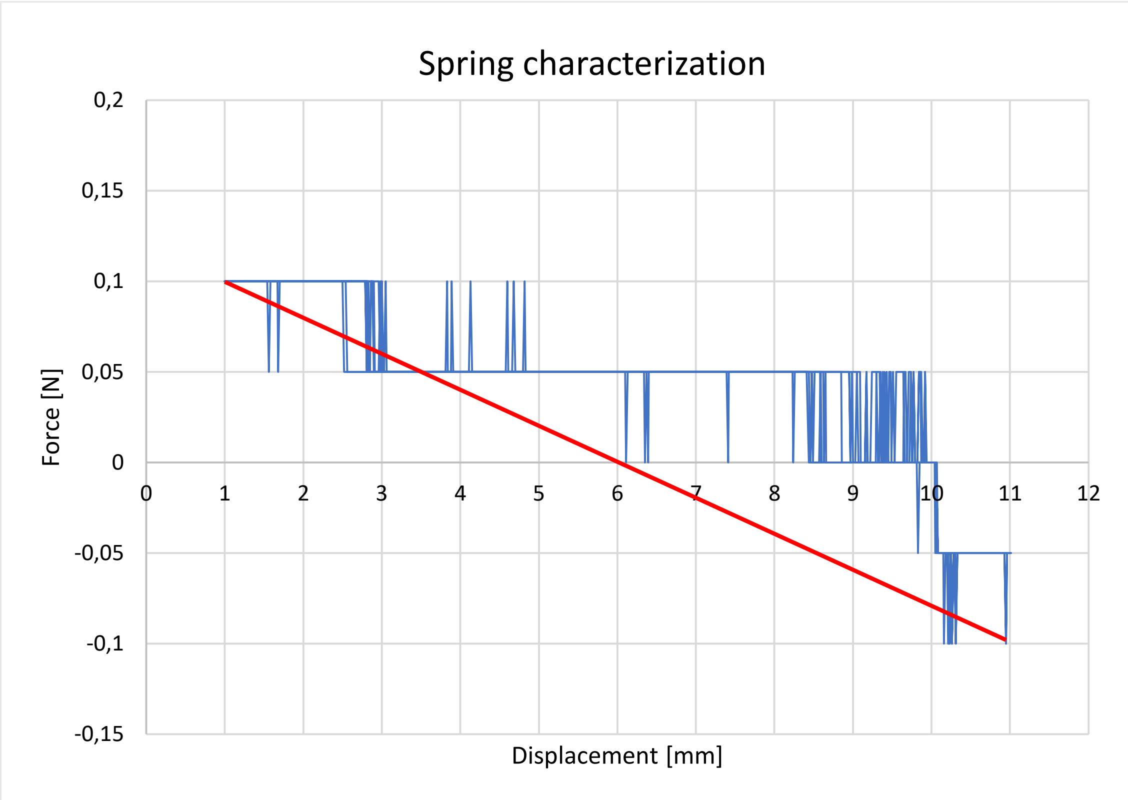

Figure 2-17: Spring stiffness characterization valve #2

The previous experimental result, if compared with the theoretical calculation from the CAD model of a different check valve, shows the same order of magnitude but slightly different values related to the specific design and application of the valve.

Theoretical value (CAD)	Experimental value (physical)
0.011 N/mm	0.020 N/mm

Table 2.6: Comparison of spring stiffnesses

These comparable results are useful to understand the generic values of spring stiffness used by different suppliers and manufacturers, this will be an important starting point for the future valve design process.
In conclusion, a small inaccuracy in the spring stiffness estimation could be due to different factors, such as sensitivity and uncertainty related to the measuring equipment, possibly present in both the loading force and spring compression measurements. At the same time random and human errors might slightly influence the experimental results.

Data analysis for valve *#1*:
A similar test was successively performed on a different physical valve coming from another supplier to obtain other experimental results for the benchmarking activity.
Using circa the same testing procedure explained above the test was carried out imposing a maximum spring displacement below 9 mm, having this spring a lower free length, and a minimum load of 0.15 N to start the spring deformation.

The linear approximation of the compression test results is reported by the red line in Figure 2-18. A meaningful characterization was obtained with F = 0.5 N and x = 8 mm, resulting in an estimate spring stiffness of *0.0625 N/mm*, which highlights a higher stiffness with respect to the previously tested spring. Consequently, the applied force is higher and with larger margin from the load-cell sensitivity, resulting in a slope with a more linear trend.

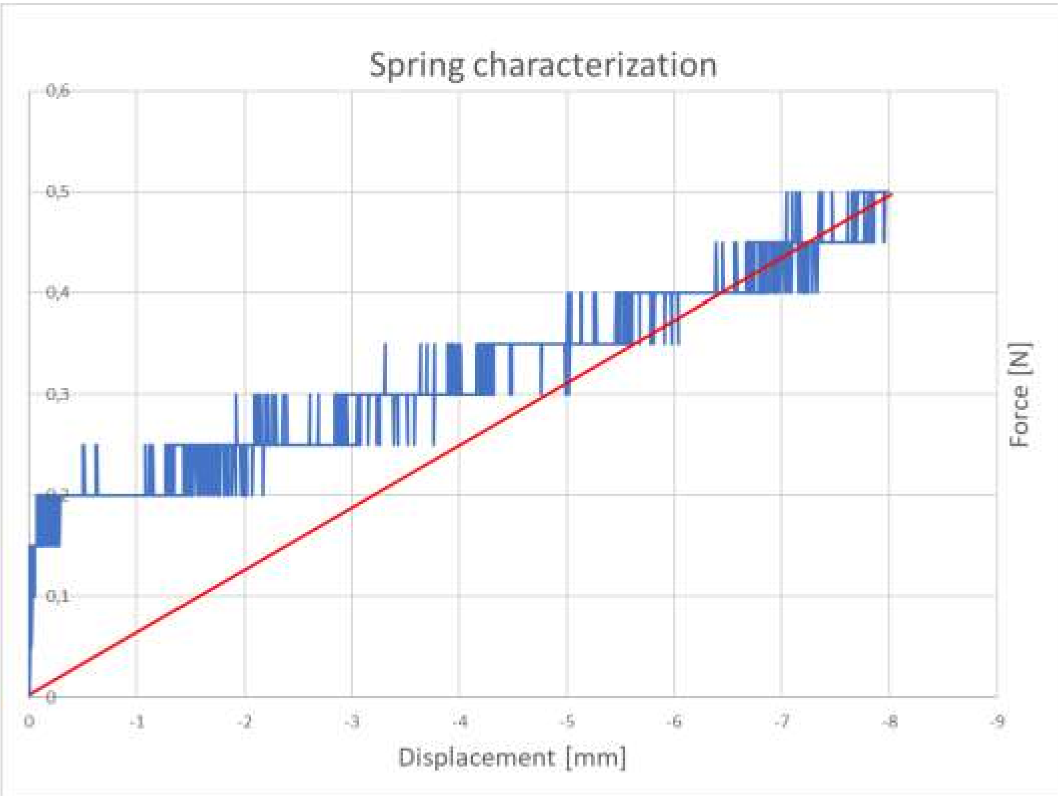

Figure 2-18: Spring stiffness characterization valve #1

2.6 Benchmarking: cracking pressure

This physical quantity, being directly related to the extremely low values of spring stiffness, required a series of bench tests and consequent trial and error procedures to be estimated; all the testing methods are explained in the following sections.

- Air-water test in water tube

The open circuit test was performed with the valve immersed in water and connecting an air pump at its inlet.
Being the minimum pressure by air pump around 40 mbar, the valve immediately opened with the air flow releasing air bubbles inside the water (pictured in Figure 2-19), meaning that the cracking pressure must be lower than the above-mentioned value and therefore other tests will be carried to obtain a meaningful result (iterative process).

Figure 2-19: Air-water cracking pressure test

- Direct measurement method

Equipment:
pressure sensors upstream ($p1$) and downstream ($p2$) of the valve;
sensors sensitivity 0.01 bar .

Methodology:
apply $p1_{min}$ to start fluid stream through the valve, which causes an increase of pressure at the outlet downstream of it ($p2$>0).

Results:
In this case the cracking pressure value $p1_{min}$ was measured by the sensor with a high uncertainty, since the instrument's sensitivity is comparable or higher than the cracking pressure to measure: $p1_{min} \cong 10$ mbar ± 10 mbar (system sensitivity error).

For both the valves under study the low spring stiffness causes the immediate opening of the valve, as soon as the flow starts at extremely low-pressure levels, therefore this test resulted in very unprecise or out of scale results. Other experimental methodologies will be tried out.

- Water column test

Methodology:
Connect a water column to the valve inlet while its outlet is open (Figure 2-20).
Gradually pour a small quantity of water inside the water column. The valve is closed until the pressure by the liquid column height exceeds the closing force by the spring on the plunger and the liquid stream starts.
The following relationship, coming from Equation 4, holds:

$h_{inlet} = p_{inlet} \rightarrow 1\ cm = 1\ mbar$

Results:
The valve opened with a liquid height of roughly 5 cm, corresponding to a pressure around 5 mbar. This has to be considered as an approximate experimental result that will be compared with an alternative theoretical result, calculated in the next sub-paragraph, since the previous experimental tests were useful just to estimate the order of magnitude of the cracking pressure.

Figure 2-20: Cracking pressure through water column method

- Theoretical calculation (forces balance):

The final alternative method was related to the force balance on the closing plunger: the cracking pressure was calculated knowing the cracking force necessary to overcome the spring force that closes the valve, preventing the liquid flow.

The flow area is calculated from the valve inlet's internal diameter D_{in}, directly measured on the physical product, that is equal to the area on the piston.
The spring stiffness was experimentally measured in the previous paragraph of the benchmarking, the resulting values K_{spring} are 0.065 N/mm for the first one and 0.020 N/mm for the latter.
From that it's possible to estimate the spring force that balances the inlet pressure to just open the check valve, using for example a small spring deformation x of 1 mm.

$$S = \pi \frac{D_{in}^2}{4} \text{ [mm}^2\text{]}$$

$$F_{spring} = K_{spring} \cdot x \text{ [N]}$$

Finally, the cracking pressure is calculated as the ratio between spring force and piston area.

Equation 8

$$p_{cracking} = \frac{F_{spring}}{S} \text{ [MPa]}$$

Converted the pressure value into mbar knowing that *1 bar = 10⁵ Pa*.

The theorical results from the previous calculations are summarized in Table 2.7, they show how these pressure values are extremely low, and therefore not directly measurable with the available instruments.

	Valve #1	*Valve #2*
D_{in} [mm]	12.5	*20*
S [mm^2]	123	314
F_{spring} [N]	0.0625	0.020
$p_{cracking}$ [mbar]	**5.1**	**0.64**

Table 2.7: Cracking pressure theoretical results

2.7 Benchmarking: bursting pressure

Equipment:

- Oil pump to increase pressure, up to maximum above 10 bar (in High Pressure test).
- Air pump to increase pressure (in Low Pressure test below 4 bar).
- Burst protection chamber for HP test.
- Water tank / tub filled with water for air-water leakage tests (only in LP test, Figure 2-22b).
- Protective screen above water tub for LP test.
- Air tap to regulate air flow and pressure.

Methodology:

- Low Pressure (LP) test:

A simplified scheme of the overall layout in reported in Figure 2-21. The pump is needed to increase pressure inside valve by closing the air tap at the valve output (pictured in Figure 2-22), up to appearance of air bubbles in the water tub due to external leakages of valve or stop the test when the pressure of 4 bar is reached, for safety reasons, measured by pressure sensor of the air pump at the inlet of the system.
Once this pressure value is reached open the air tap to vent the system and reduce the pressure inside the valve.

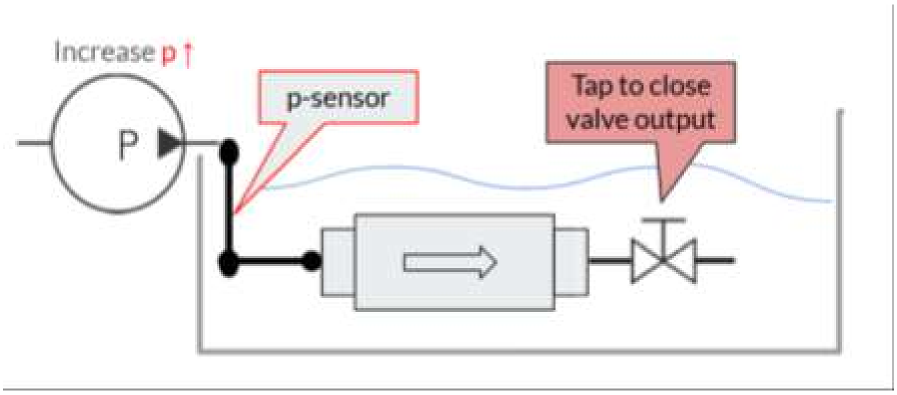

Figure 2-21: Scheme of bursting pressure test

Leakages may also be measured with air-air tests to guarantee a higher safety margin with respect to tests using coolant, applying a safety factor around 2-3 times the maximum working conditions of the product.

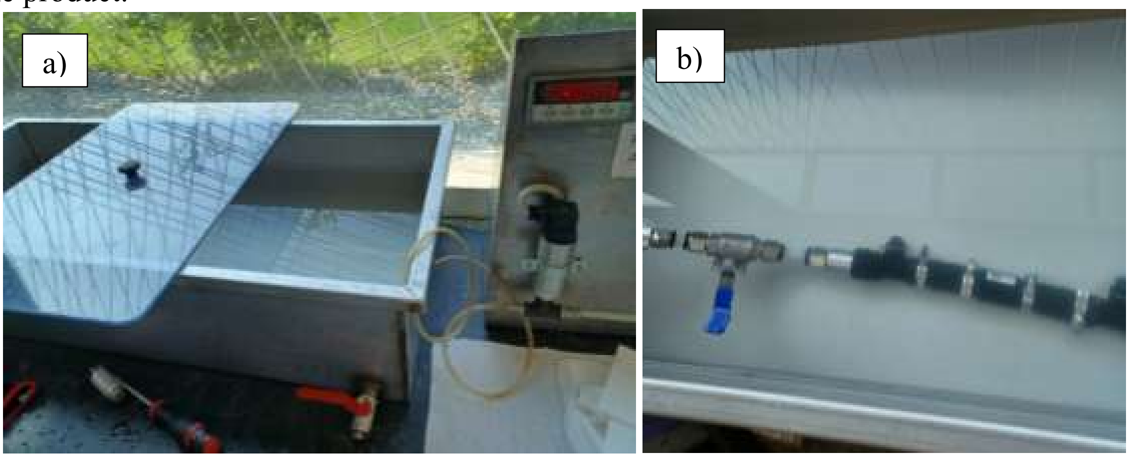

Figure 2-22: Low pressure test: a) system setup; b) valve and air tap

For both the valves under test resulted in no bubble appearance inside the water tub, up the maximum pressure level prescribed (4 bar, as possible to notice on the display in the top-right corner of Figure 2-22a), therefore passed by both the valves under study.

- High Pressure (HP) test:

In this case lubricant oil is injected in the valve whose outlet section is blocked to increase pressure inside its body, up to 10 bar or more, until explosion of valve body in correspondence of the weaker section of the wall or more easily in case of assembly criticality.
Since this is a destructive test, this operation is performed automatically inside a test chamber. Measure limit pressure value just before valve's destruction to identify the bursting limit.

2.8 Benchmarking: product mass

As last activity of the benchmarking analysis the mass of each valve and of each internal element composing them (spring and piston) was measured, in facts it is an important parameter since its footprint on the cooling system must be as low as possible while respecting the performances and requirements analyzed so far.

The measurements results are reported in Table 2.8 for sake of completeness:

	Valve #1	Valve #2
m_{body} [g]	30	18.7
m_{piston} [g]	2.2	2.1
m_{spring} [g]	1	0.5
m_{TOT} [g]	33	21.3

Table 2.8: Benchmarking of valve masses

2.9 Transparent valve characterization

Following the benchmarking related to the main requirements and parameters expressed so far, a final experimental activity was performed to characterize the displacement of piston and spring inside the valve body as a function of the volumetric flow rate imposed through it.

The internal physical components (piston and spring) were taken from the test valve #1 that was sectioned in the previous benchmarking work to measure their mass.
A testing prototype was designed starting from the available technical drawing of valve #1 and from the physical measurements on the product under test. The CAD design included an O-ring seat for a leakproof assembly, realized through bolts and nuts connection for simplicity and possibility to dismount the inlet from the body of this testing prototype.

This new CAD prototype was printed by using a 3D printer with a transparent resin material, the internal components (visible dark plastic elements) were positioned inside and the assembly was connected to the testbench equipment through pipes and connectors, as pictured in Figure 2-23.

The test was performed slowly increasing the volumetric flow rate imposed by the pump through the system and observing the consequent displacement of the piston and spring, that resulted to vary almost in a linear way with the flux as shown in Figure 2-23:

a) Closed valve until $p < p_{cracking}$ for low values of coolant flow (Q from 0 up to 2 l/min);
b) Equilibrium condition with the plunger displaced more than half-way when the pressure is balanced by the spring force, with intermediate flow rates (Q in the range of interest 3 -10 l/min);
c) Fully open valve when a static condition is reached, obtained for higher flows and pressure levels (approximately Q > 10 l/min).

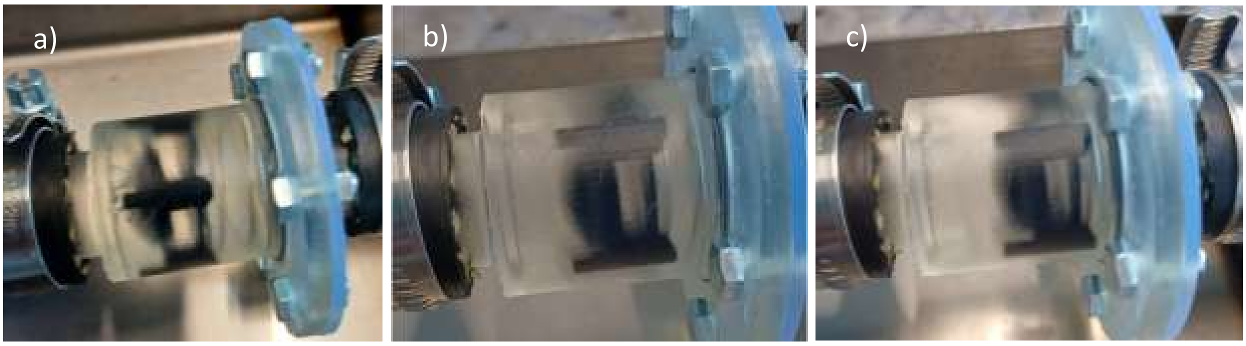

Figure 2-23: Transparent valve configurations: a) closed, b) equilibrium, c) fully open

These outcomes showed that the valve works between more than half-way and full displacement configurations in the flow conditions given by the requirements, in particular this consideration will be a starting point for the CFD model that will be used to simulate the new designed valve prototypes.

3 Valve design

3.1 Components sizing (definition of components characteristics based on system working / surrounding conditions)

The information and data coming from the previous benchmarking activities will be used in this chapter for the design modeling of the new component prototype.

As a first step a pre-dimensioning was done considering these main parameters:

- Functional quotes of the product, in particular inlet and outlet outer diameters (D_{in} , D_{out}) that must be taken from standard pipes dimension to standardize the product mounting for an easy installation inside the cooling system but also the diameter of the valve central body (D).

- Overall dimensions, that should be reduced to have lower footprint inside the cooling system; in particular a reduced length of the central body results in a lower product length and range of deformation of the spring (L below 80 mm).This has also an advantage from a fluid dynamic point of view; according to the theory a lower pipe length will result in lower pressure gradient through the valve body (Equation 9).

Equation 9

$$\Delta p \propto \frac{L \cdot v_{avg}}{D^2}$$

- Limited walls' thickness ($t \leq 3$ mm) to reduce weight and cost of the final assembly, in facts for this study case there is no need of high mechanical performances since the check valve is used in low pressure conditions.
  Particular attention will be paid to the assembly interface, whose design changes according to the feasible manufacturing processes that will be discussed and chosen for the product in the following chapter 3.2.

- Another key aspect to consider was the design of the valve body flow area to reach the main functional targets, such as no obstruction to obstacle and deviate the stream path, no turbulence and reduced pressure drops, obtained with wider diameter in the central body of the valve, in facts larger openings provide less resistance to the fluid's flow and result in a lower average speed (v_{avg} in Equation 9), which was shown being favorable for pressure loss reductions .

That said, the design of the internal components must be carried out as a consequence of the valve geometry.

At first the **spring** was dimensioned considering the geometry and desired characteristics of the product, following different possible paths:

- CAD design: evaluate the desired spring stiffness from the mechanical properties of the material chosen (usually stainless steel), spring mean diameter *D*, coil diameter *d*, number of active coils *n* and applying the above reported Equation 6.
- Choose from catalogue of suppliers to adapt our geometry to a standard product with lower cost; since both the internal and external spring diameters are known, it should be possible to choose appropriate spring with given spring rate. This hypothesis resulted not feasible since all the products on the market had a too high stiffness for the application under study.

The spring prototypes under design must ensure mounting in all directions, also vertical.
For that reason, an estimation of the spring stiffness can be obtained from a force balance estimation: it must balance the weight of closing piston, mass of coolant inside valve inlet and connected pipe vertical in system to avoid the backflow of coolant when no pressure is applied inside the system.
In addiction the design of valve body and spring seats has to ensure the correct pre-deformation of the spring inside the assembly to balance the total force from the above calculations.

Afterwards it's necessary to verify the valve cracking pressure in each case, considering the chosen spring stiffness and the geometry of the inlet area, as estimated before (Equation 8). It's important to keep this quantity at low values, in the order of few millibars as shown by the outcomes from the benchmarking, to allow easy coolant flux, low resistance and pressure loss caused by the piston.

A possible design of **internal plunger** was carried out considering the importance of modularity to allow the use of the same valve body to mount different closing elements with disparate designs:

- Proto#1: Simple half-sphere-shaped piston in which the first sealing action is due to tangential contact between ball and valve entrance seat while the second one by a flat rubber ring that leans on the outlet wall of the central body.
- Proto#2: rubber piston head designed just for the specific study case, to guarantee a direct sealing action on the inlet wall chamfer.
- Proto#3: Rubber piston with a more complex and fluid-dynamic shape to analyze its pressure loss performances and compare it with the simpler piston performances; this process has been performed and described more in details in the CFD chapter 4.4.

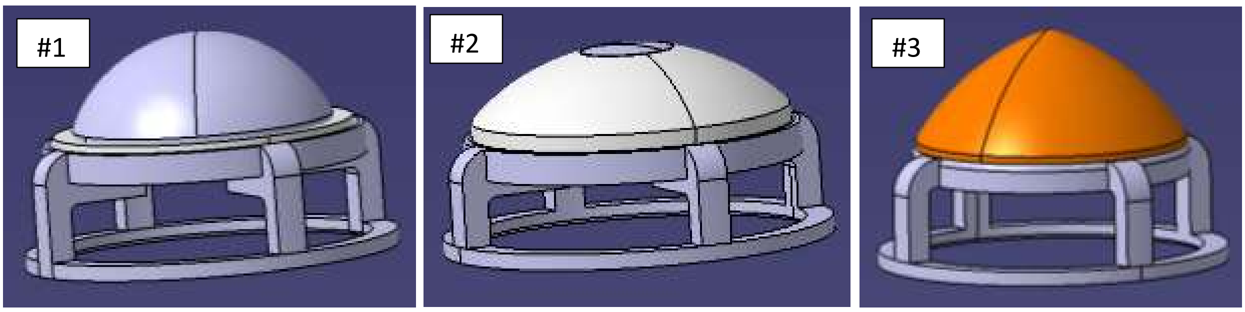

Figure 3-1: Piston prototypes #1, #2 and #3

For each of the hypothetic prototype the overall tradeoff between performances, sealing action, pressure drop, assembly complexity and cost has to be examined.

3.2 Material and assembly process selection, 3D modeling of components and assembly (CAD)

3.2.1 Material selection

The materials used for this application are mainly thermoplastics, due to the fact that the valve is used in a low temperature loop and its material is not subjected to high temperature gradients or excessive mechanical stresses.
In particular ***PA66 GF30***, a 30 % glass fiber reinforced polyamide, is a suitable option used by some competitor companies for this kind of applications since it offers higher strength, rigidity, creep strength and dimensional stability than the standard unreinforced polyamide (PA 66).
Before use this lightweight material has been heat stabilized and hydrolysis resistant to make it refractory to many oils, greases and fuels that could possibly be encountered during its operational life.

The above-mentioned material is obtained through an injection molding process, as schematized below in Figure 3-2 [6]:

- A matrix of molten plastic (*PA*) is mixed with the glass fibers (*GF*), whose percentage content, fiber distribution and orientation depend on the application type and requirements. The glass fiber is mixed in solid state, since its melting temperature is above 500 °C.
- Subsequently the mixed materials are pressed and transported by a screw and finally injected into a mold cavity under high pressure conditions to give the desired shape to the part.
- Finally, the molten plastic matrix is rapidly cooled to solidify; afterwards the mold is open and the finished part is extracted.

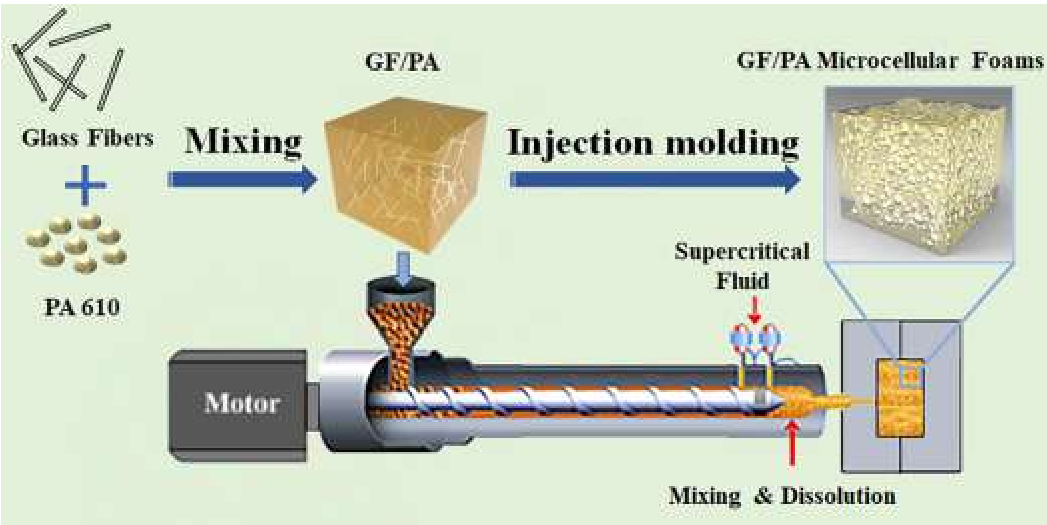

Figure 3-2: Scheme of GF-PA injection molding process

When needed, a possible mechanical strength improvement could be obtained by changing the percentage of glass fiber content, with an increased quantity, up to 50% or more, for increasing

stress and requirements on the material's performances according to its applications, but this is not the case for the system valve under study.
The main drawback of the presence of a certain percentage of glass fibers inside the polyamide matrix is its very low and difficult weldability; being the glass fiber randomly distributed, its presence on the external surface of the part would cause a weaker and not waterproof joint, since the glass fiber doesn't melt at the temperature reached during the welding process of the plastic materials.
A further disadvantage of this composite material is its cost: glass-filled nylons are more expensive than standard unreinforced polyamide, in fact these blends can cost up to 50-100% more due to the additives and the additional processing.

In general, the *PA66 GF30* is considered a good compromise between low production cost and mechanical/thermal performances, but for this specific study case, in which both the thermal and mechanical stresses are very low, the possibility to use a standard unreinforced polyamide, such as ***PA 66*** or similar, will be investigated.
This choice is also strictly linked to strategic and economic reasons, due to the variable cost of the material depending on the volumes traded with the company's supplier.

The mechanical properties have been taken from the software settings used for the FEM analysis (Solidworks) and they are here summarized and compared [7].

	PA66	**PA66 GF30**
Elastic modulus [MPa]	2620	5500
Shear modulus [MPa]	970	319
Yield strength [MPa]	103	91
Density [kg/m^3]	1120	1370

Table 3.1: Material properties comparison

Finally, the material marking might also be printed on the body of the valve as an additional indication for the customer and in addition the European regulations imposes the marking on plastic materials for recyclability issues.

3.2.2 Assembly process selection

Other important information for the manufacturing of this process is related to the production method used for its final assembly. Thus, in this section of the thesis work the main feasible assembly processes for thermoplastic materials are summarized, highlighting the pros and cons for each of them.

3.2.2.1 Rotary friction welding

Rotation welding process, or more precisely Rotary Friction Welding, is a solid-state process in which one part is rotated at high speed and is pressed, along its axial direction, against another part that is held stationary. The resulting friction between the parts heats them, causing them to forge together forming a unique body [8].

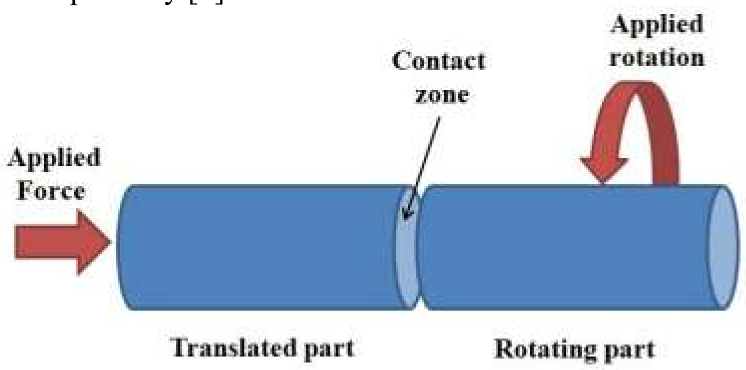

Figure 3-3: Simple scheme of rotary friction welding

General features: rotating speed 1200 - 3500 rpm, welding pressure 0.5 - 2 MPa.
This process is very efficient for pieces made of thermoplastic material and with a tube or circular-section shape, such as the valve flanges and body, all made of polyamide PA6.6 and with rotationally symmetrical joining surfaces around their common axis of rotation.
Welding is a suitable process on the valve for airtight connection, to avoid leakages or bubble formation under normal operating conditions.

To guarantee a correct welding the inlet flange must have a small interference with the valve's body, in this way this additional material melts with the friction heat, spreads uniformly inside the groove (interface slot) thanks to the high-speed rotation and creates a uniform joint in the interface between the two parts. The two initial bodies, made of the same material are joined together and become like a single airtight body without any visible separation between the materials and with no need of the addition of external elements such as clips, O-ring or seals.

The main advantages of this technique are:
Precise and permanent welding without additional weight, cost and space of sealing components.
Simple and permanent installation of the final product since it's useless to provide a dismountable joint, no need of maintenance for this non-complex product, just spring and plunger inside the valve body.

Some drawbacks are related to the high initial investment for the machinery, that must be very precise to guarantee the leakproof assembly. In addition, the total cycle is longer if compared to other simpler processes, in facts it also includes the solidification time of the molten material (around 10 seconds in total).

3.2.2.2 Ultrasonic welding

Ultrasonic welding is a solid-state joining process that uses mechanical vibrations to soften or melt a thermoplastic material, such as the polyamide under study, at the joint interface.
The parts to be joined are pressure and subjected to ultrasonic vibrations, usually at a frequency of 20–40 kHz. The mechanical energy is converted to thermal energy by surface friction that melts the plastic and welds the two parts together creating a strong and permanent bond [9].

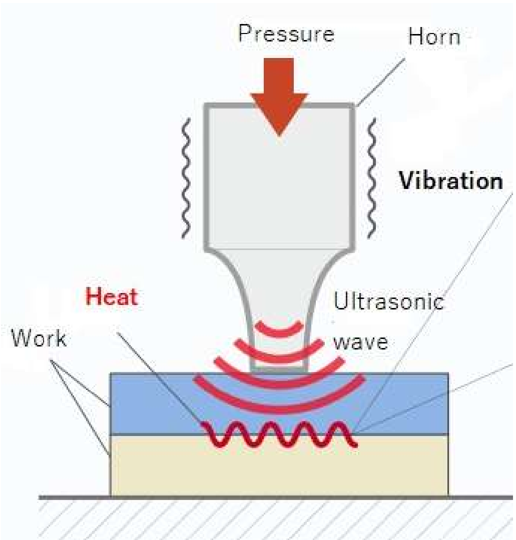

Figure 3-4: Simple scheme of ultrasonic welding

Some of the advantages for ultrasonic welding are:
Low cycle times (around 1 second or less) and therefore high-volume production.
Clean process without need of additional filler material.
Automation and flexibility of the process.
Excellent surface finishing with minimum heat affected zones and low thickness weld.

The main drawback is due to the high initial investment: basic ultrasonic welding equipment is significantly more expensive than traditional welding equipment, especially if highly automatized. Furthermore, ultrasonic welding is limited to simple and normally flat surfaces of the mating parts.

3.2.2.3 Interference coupling / joining with clips

Coupling with interference or clips allows to get the final product by pushing the parts' interlocking components together through their geometry design.

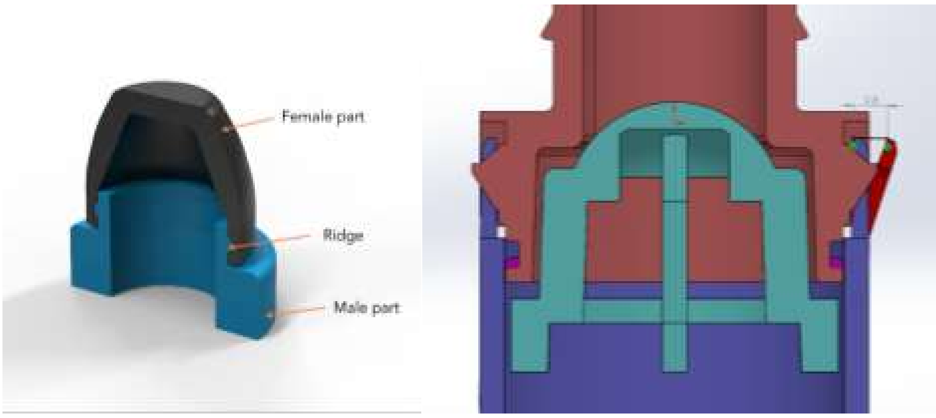

Figure 3-5: Example of interference/clips couplings

Pros:
Reduced insertion force, fast installation and reduced cycle time through simple interlock.
Possible to mount/dismount product in case of needed for maintenance (very rarely if designed for that specific purpose).
Automation in the process for high volume production.

Cons:
Lower pressure seal if not properly designed, possible leakages at high pressure (must respect specifications during the tests, for example the bursting pressure).
Additional rings and gaskets to avoid leakages, implying additional length to the component (O-ring at least 1 mm extra thickness, also additional groove for the mounting).
Additional cost and weight. Need of a centering mechanism for correct assembly of the mating surfaces.
More complex design for the shape of mating parts. Mechanical properties of the clips must satisfy mechanical requirements.

During a design process the hypothesis of **clip** assembly was investigated by designing two prototypes, both having a similar shape of the mating parts; an example is depicted in the CAD prototype of Figure 3-6.

This type of design is composed by [10]:
- deformable *outer seat* on the valve outlet part;
- stiffer *inner clip* on the inlet that interlocks the seat by mean of a *mounting ramp* surface, designed with a limited slope to reduce the mating force.
Instead the dismount action is not possible since the interface between the designed mating elements has no angle and their faces are in contact on the same plane.

As a way to facilitate the deflection of the clips towards the outside during the assembly, an *external notch* was designed to reduce the material that must be deformed at the root of each clip but still guaranteeing structural stability.

In order to respect technical requirements related to the correct and simplified assembly through a centering and mating design, *guiding walls* on valve body have been added to the prototype for a precise mating with the protrusions on inlet, necessary to guide the assembly and ensure correct aligning of clipping elements.

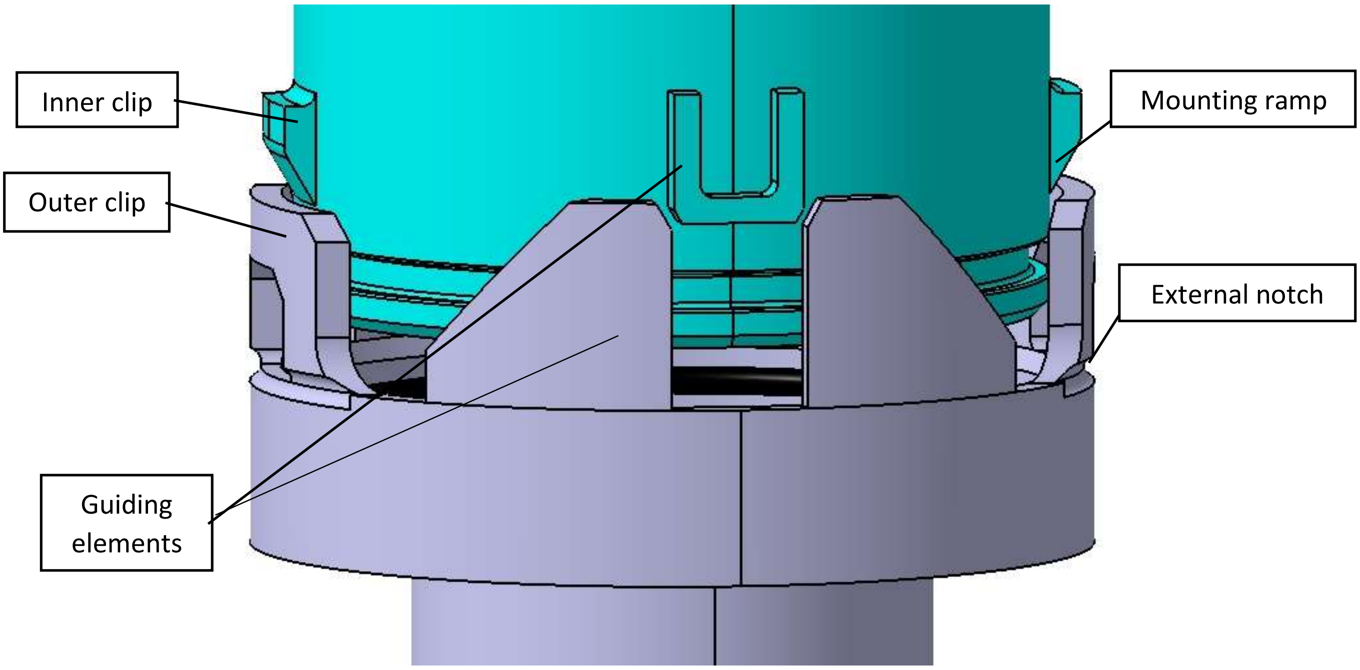

Figure 3-6: Clip assembly and guiding prototype

- **Clip assembly FEM analysis**

After a preliminary design of the clips it was necessary to simulate the assembly by availing a Finite Element Method analysis (FEM) software, the specific tool included in SOLIDWORKS.

At first simulate the assembly process through the **deflection** of the arms, imposing the displacement to the upper edge to overcome the clip on the other body (0.7 mm deflection in the prototype under study) while the opposite extreme of the body is constrained as if fixed by the pipes in the final assembly position; a mesh refinement was applied in the critical areas where the edge fillets are present to reduce the stress concentration.
The graphical and numerical outcomes of the simulation (Figure 3-7) are used to compare local level of stresses with the yield point of the tested materials, represented by the violet color, for both a generic polyamide (*PA66*) and its fiber glass reinforced version (*PA66 GF30*), to avoid plastic deformation of the clip.

An additional simulation had to be performed to ensure the compliance to a parameter imposed by the customer requirements, such as the maximum **bursting pressure** that the assembled valve has to endure in the critical testing conditions (10 bar).
The clip arms are constrained as if the two mating bodies are mounted, a pressure is imposed on the inside surface of the valve outlet, normal to the fluid stream as represented by the red arrows in Figure 3-8. This simulation seems to be conservative because overestimates the stress on just the clips' arms, neglecting O-ring and surfaces contacts actions in the real assembly.

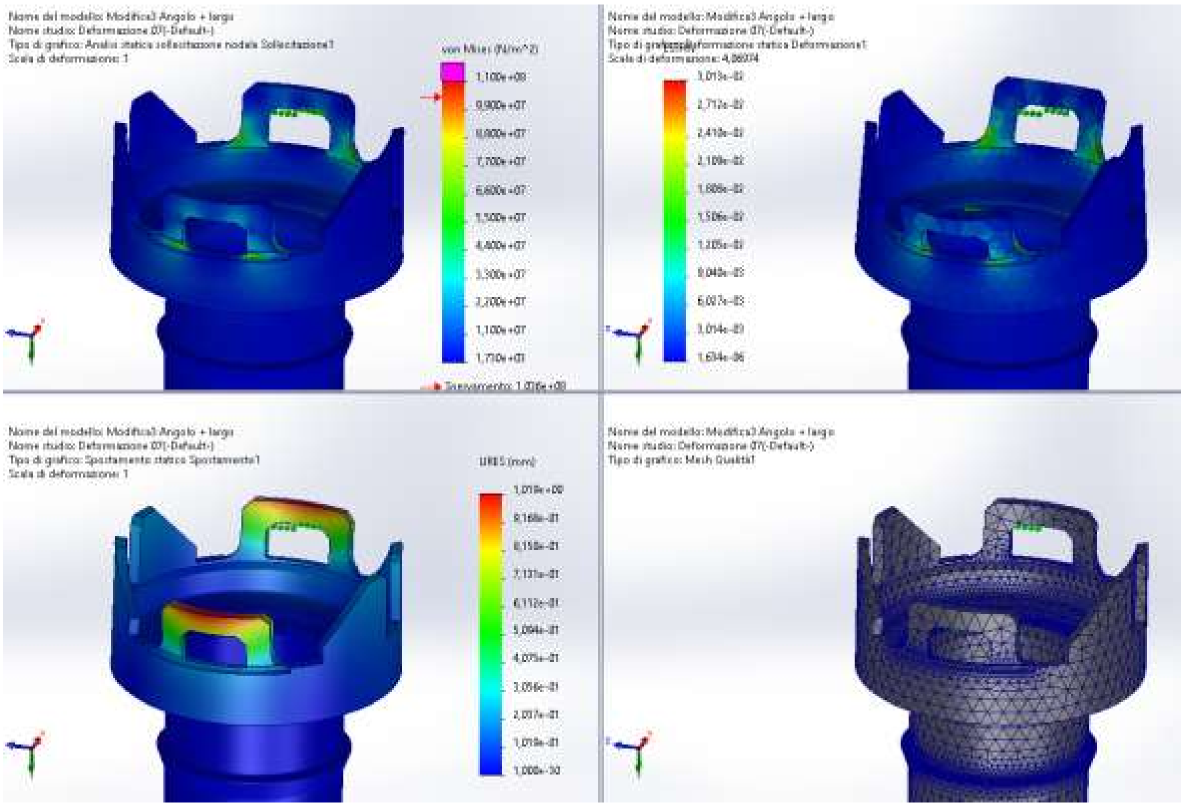

Figure 3-7: FEM analysis on clip_ assembly deflection

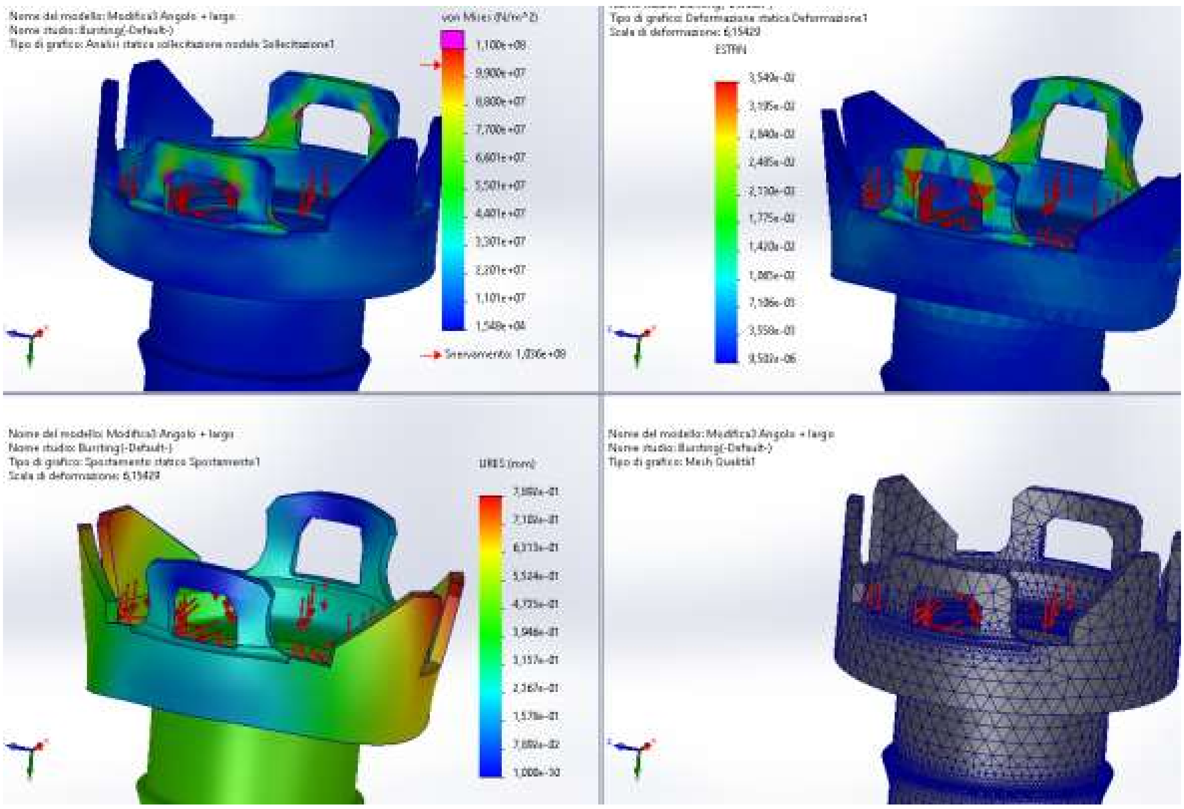

Figure 3-8: FEM analysis clip_ bursting pressure

The main outcomes of the first simulation show that the stress level in the most critical areas (green and yellow colors in the Figure 3-7 plot) are always in a range far from the yielding limit of the material, meaning that the clip deflection for the assembly is theoretically verified for this design.

The clip under bursting pressure test in Figure 3-8 was always represented in with a larger scale of deformation (6 times more) to highlight the deformed shape of the part and the resulting stresses in those areas.
Also this latter simulation gave positive results as the critically stressed areas resulted being very localized and not too high since the wall thickness in the clip corner was increased for safety.

More simulations were performed to compare the performances of the 2 possible materials, *PA66* and *PA66 GF30*, whose mechanical properties were reported in Table 3.1.
A clear difference in the results is due to the difference in yielding strength of the materials, resulting in much larger critically stressed areas in the glass fiber reinforced prototype.
For that reason, the final choice of the material seems to be more oriented towards a standard polyamide nylon material, in particular PA66.

This prototyped required an additional design complexity related to the **O-ring** choice from the catalogue and dimensioning of its seat according to the standard dimensions and working conditions for the specific application.
In particular, this choice could lead to an increase in the outer diameter of the valve to facilitate the assembly process, but with an overall limited impact on its footprint, which is one of the main functional requirements.
Important additional considerations: increase diameter to guarantee a larger clearance to prevent the pinching of the O-ring between the 2 mating parts during the mounting operation.

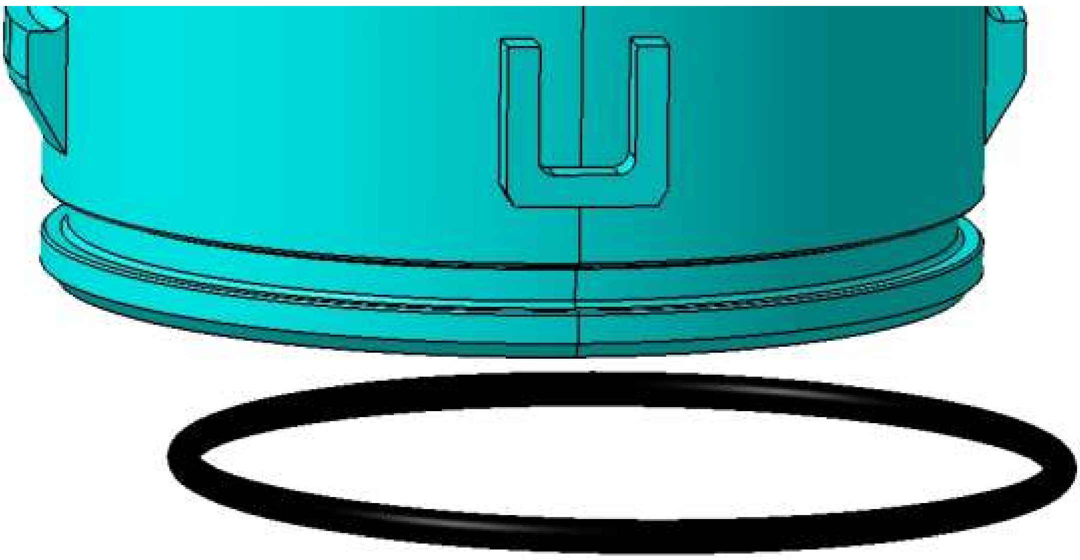

Figure 3-9: Detail on O-ring groove CAD model

3.2.2.4 Mechanical fastening

This assembly method allows to obtain by using some sort of fasteners, such as screws, rivets or bolts and nuts.

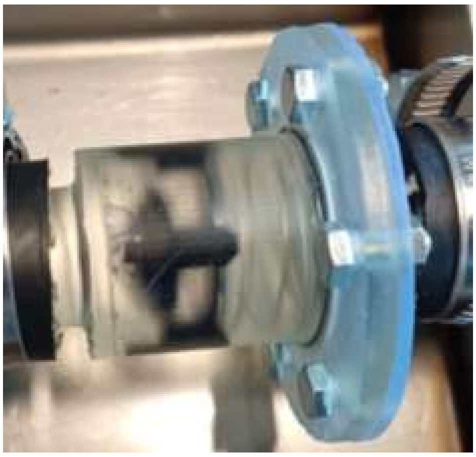

Figure 3-10: Example of mechanical fastening

Pros:
Dismountable interface in case of need. Standard dimensions of fastening elements.

Cons:
Increase in product volume and design complexity because of holes and seats for the fasteners. Slow and complex assembly process. Need of additional sealing in the assembly interface. Additional material of metal mechanical fasteners resulting in extra cost and weight, so not suitable for the low weight and low complexity study case, such as the check valve that doesn't require internal maintenance once mounted inside the cooling system.

3.2.2.5 Gluing or adhesive

A permanent joint is obtained through a layer of glue of adhesive material between the mating parts to be joined.

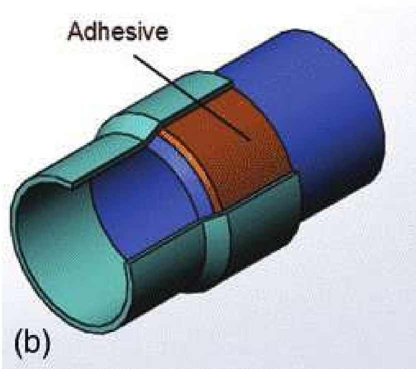

Figure 3-11: Example of adhesive assembly

Pros:
This assembly technique has the flexibility to join all materials, also dissimilar materials if a glue with the proper chemical properties is employed. Also suitable to joint complex shape interfaces.

Cons:
Long cycle time in the assembly process, in facts the solidification and curing time of the glue has a large impact on it.
Design of parts to increase mating surface for the glue application.
Chemical compatibility and possible degradation of adhesive properties in presence of solvents or chemical agents, such as the glycol of the cooling fluid inside the system under study.

These requirements on the assembly have some tolerance in terms of maximum air leakage, examined through an air-air test at increasing pressure levels.
Air-air tests are much more severe than coolant ones, since the liquid is characterized by a higher viscosity with respect to the air, a higher fluid resistance to flow resulting in lower external leakages under the same testing conditions.

3.3 Final design selection

The final choice of the assembly method, among the most feasible ones listed and explained so far, will be made according to some key parameters that can be divided into 2 main categories, as summarized in the following tables (Table 3.2 and Table 3.3) with some indicators where the plus signs "+" indicate an advantage while the minus "-" a pain point.

The technical and functional ones are about:

1) Complexity of the assembly and technical feasibility for the geometry under study
2) Number of components and design complexity of the interface
3) Final footprint and mass of the product, that has to be minimized.

Method	Complexity	Interface design	Footprint
Roto-welding	+	+	+
Ultrasonic welding	-	+	+
Clips	-	-	+

Table 3.2: Assembly methods- technical comparison

Others are instead related to the cost and time of the process:

1) Initial investment for the machinery
2) Cost of the working station, depending on the complexity of the assembly operation to be performed
3) Cycle time and energy consumption.

Method	Initial investment	Assembly cost	Cycle time
Roto-welding	-	+	+
Ultrasonic welding	- -	-	+
Clips	+	+	+

Table 3.3: Assembly methods- time/cost comparison

This brainstorming activity was necessary to identify and compare all the technical/economical aspects from the above-mentioned assembly methods and get to a final choice for the manufacturing process and design for the check valve under study.
The final candidate chosen for a possible industrialization was the clip assembly with circular shape, containing all the parts designed so far: spring, O-ring, piston support and rubber head as pictured in the assembly cross section of Figure 3-12.

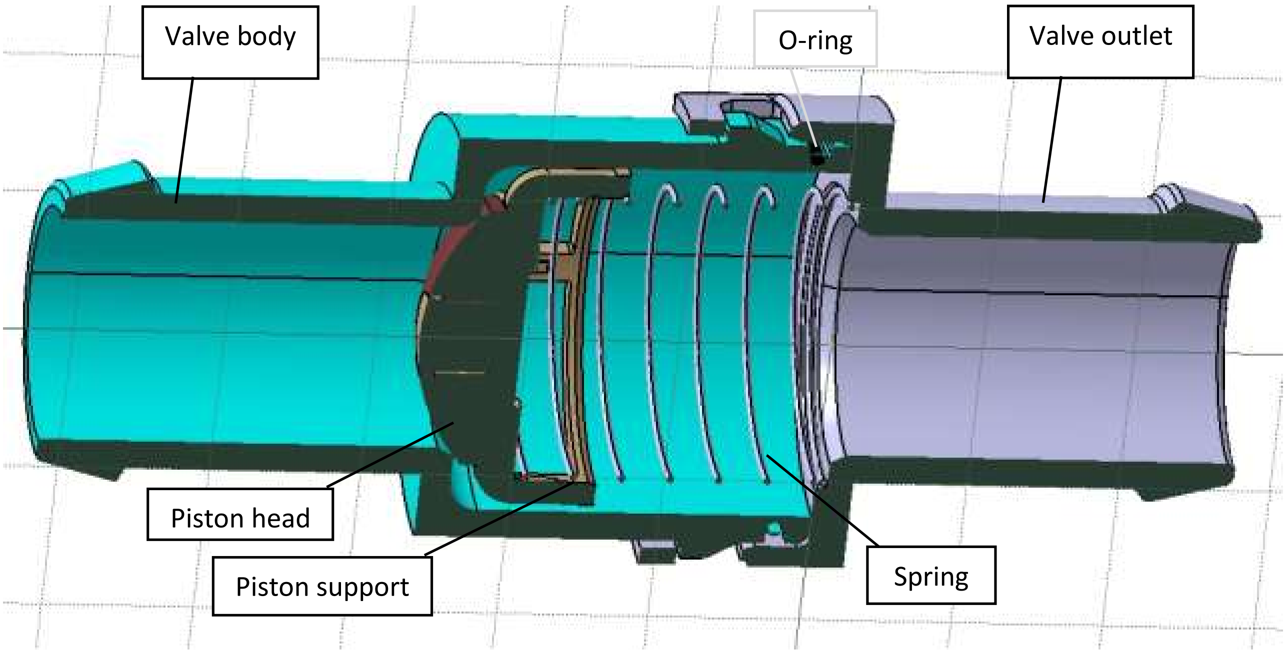

Figure 3-12: Final check valve assembly 3D cross section

For sake of clarity and completeness the technical drawings of all the components designed are reported in the Appendix (A2_Technical drawings) at the end of this thesis work.

All the parts shown above, represented by both a 3D body and a technical drawing, have been modelled considering geometrical tolerances and tolerance chain (through stack-up calculations) inside the assembly to guarantee the needed clearance or interference in the interfaces (both axial and radial) between the parts composing it, in particular in the clips interface and O-ring seat regions.

The design process includes the creation of a reference part number for each body part reported on the corresponding drawing, together with the revision number and other useful information such as material, estimated mass of the body and eventual surface treatment coating.
This procedure is necessary to encode all the parts CAD documents and technical drawings in the company database.

The assembly of final product includes a bill of materials (BOM), table reporting the comprehensive inventory of the bodies, parts and components, as well as the quantities of each needed to manufacture the final product assembly. This aspect is crucial for the company to estimate the amount and cost of materials, for planning purchases, ensuring the availability of parts and avoiding production delays for the product.
Final product's drawing also reports some necessary information for the assembly process, the main functional specifications and performances of the valve, in particular the pressure loss chart.

All the drawings report the indication of "prototype" state of the components and assembly, meaning that they could still be subjected to geometry revisions and modifications.

In the employed drawing software (CATIA V5) the following terminology is reported:
each body is represented in a CATPart, the product assembly in a CATProduct and the technical drawing by a CATDrawing.

4 Check of valve sizing thanks to CFD simulation

This part of the thesis work investigates the stream velocity and pressure values across the valve using Computational Fluid Dynamics as a tool. All the steps followed and main results are reported in the following sections.

4.1 CAD model creation

Simulations on the valve prototypes designed so far will be performed by availing the COMSOL Multiphysics software [11], which considers all principles of Multiphysics and solves the Navier-Stokes Partial Differential Equations (PDE) to post-process the results and get the desired outcomes from the steady-state flow simulations.

Starting from the designed prototypes, modelled during the iterative process described in the previous chapter, some CAD models were created for the CFD simulations. To reduce the complexity of the mesh, computational time and obtain clearer results of pressure loss, the spring inside the valve was not considered in the models (1st simplifying hypothesis).

The fluid volume inside the valve was discretized extracting the empty volume within the existing valve parts; in practice a negative of the product was created, in which the empty space available for the fluid flow is represented by a control volume to be meshed while the piston and rubber ring are represented as empty space, as pictured by the cross section of the valve in Figure 4-1.

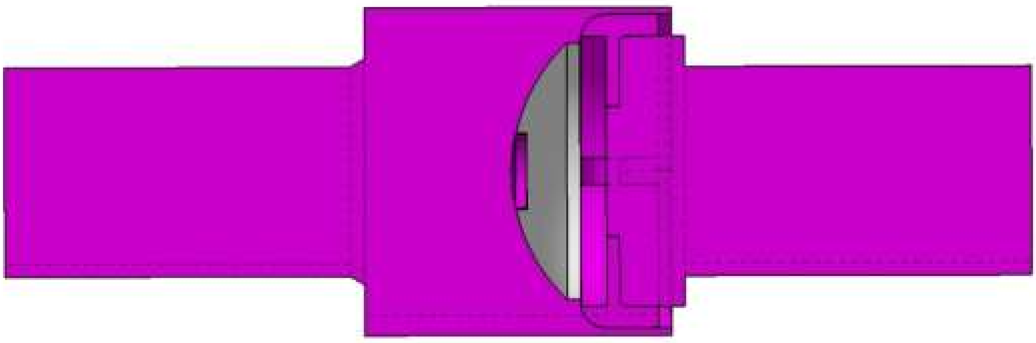

Figure 4-1: Fluid domain control volume, fully open valve

From the available geometry data, volume flow rate parameter and working fluid properties and availing the continuity equation, it's possible to evaluate the mean velocity of fluid through a cross section, that depends on the value of the imposed volumetric flow rate and area of the flux, in both the inlet (A_{inlet} with D_{inlet}=16mm) and body (A_{body} with D_{body}=25mm) of the valve.

Equation 10

$$v_m = \frac{Q\left[\frac{m^3}{s}\right]}{A\,[m^2]}$$

Afterwards these mean velocity values will be used to evaluate the Reynolds number (*Re*) of the flow for each of the three values of Q in both the valve's inlet and body sections.
Re is an a-dimensional parameter, defined as the ratio between inertial and viscous forces in the fluid, depending on fluid kinematic or dynamic viscosity, the mean flow speed and the characteristic length of the flow section, in this case the valve inlet length.

Equation 11
$$Re = \frac{\rho \, v_m \, l}{\mu} = \frac{v_m \, l}{\nu}$$

From the theory:

> if Re > 4200 the flux results being turbulent,
> for Re < 2100 the flux occurs being laminar
> transition phase for values in between.

The results of the calculations are summarized in the following Table 4.1.

Re (Q)	inlet	body
Q1	7791	3191
Q2	15581	6382
Q3	23372	9573

Table 4.1: Reynolds number calculations

From the theoretical results shown in the table the flux was estimated to be turbulent for any value of flow rate, which results in vortices, flow instabilities and chaotic eddies.

4.2 Boundary conditions and working fluid

The working fluid and boundary conditions have to be specified as inputs for the software solver simulations.

The outlet pressure p_2 was set to 0, since it's considered to be at ambient level before the start of the flux through the valve while the cooling system working pressure p is 1 bar, but this value changes with the flow rate in proximity of the valve as studied in this chapter of the thesis work.
Another input for the simulation is the volumetric flow rate Q that must be set for each working condition under study (5, 10 and 15 l/min), specifying the direction of fluid stream on the valve's CAD model.

The liquid coolant parameters are set according to the specification that were reported in Table 1.1: in particular the fluid composition 50% glycol, kinematic and dynamic viscosity and density at the working temperature imposed, expressed in absolute terms as 333.15 K in the software.

Finally, the wall boundary conditions were set to *non-slip* conditions. In this way the walls of the valve and the piston surfaces represent a boundary layer, on which the fluid velocity is zero because of the friction force between fluid and solid boundaries. The fluid velocity then changes from zero at the surface because of the no-slip condition to a maximum at the pipe center, therefore it is convenient to work with a mean velocity v_m.

Since the model under study was estimated to be characterized by a turbulent flux, the COMSOL Multiphysics software was set to use the *K-ε turbulence model*, one of the most widely employed two-equation eddy-viscosity model. It is based on the solution of equations for the turbulent kinetic energy K , which determines the energy in turbulence, and the turbulent dissipation rate ε, which determines the rate of dissipation of turbulent kinetic energy. The computations on this model are solved by Newton's method equations solver.

4.3 Meshing

Factors such as computational cost and accuracy requirements should be considered in this part of the work, since the maximum number of cells is limited by the computational power of the computer used.
As a first try a static fixed mesh will be used in the steady-state flow simulation on the fully open valve model for each flow rate value under test (2nd simplifying hypothesis).

An initial set of simulations was performed using a *coarser* tetrahedral mesh to obtain an acceptable accuracy of the solutions for the comparison of the prototypes performances; automatic remeshing was chosen so that the software automatically refines the mesh in those areas where the geometry in more complex or the flow area undergoes some section changes, so as to investigate more precisely the turbulences in those physical regions of the control volume, as depicted in Figure 4-2.

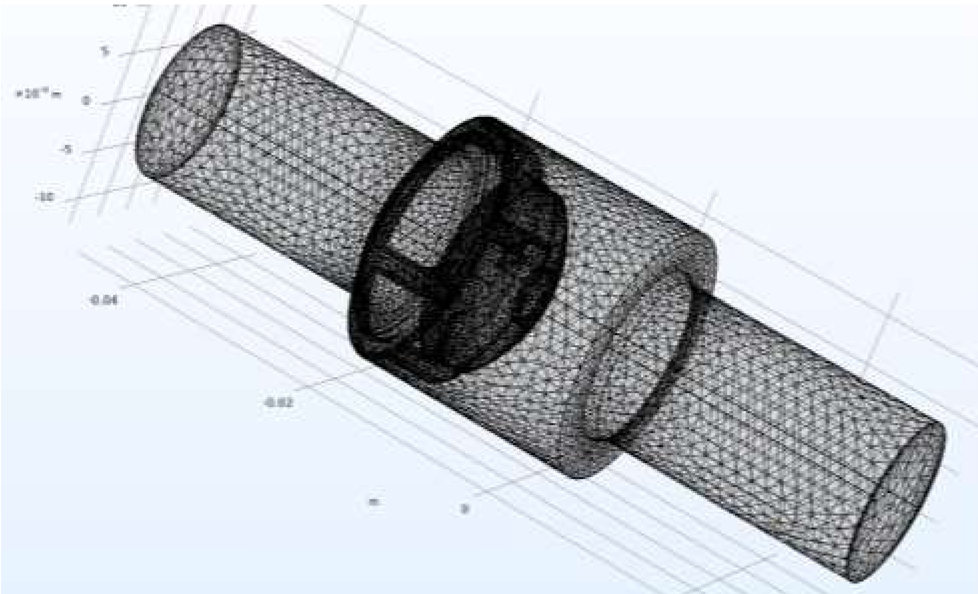

Figure 4-2: Coarser mesh example

Once the comparison of the prototypes is completed and the best candidate is chosen a further refinement of the mesh is performed to carry out more detailed simulations, but since the outcomes in terms of delta pressure were comparable, the previously tested coarser mesh was kept to reduce the computational power and time without worsening the accuracy of the results that seemed to converge.

4.4 Simulation's results

This section is dedicated to the post-processing and visualization of the main outcomes of the simulations, in particular pressure and velocity fields, pressure drops measurements and flow streamlines plots obtained from the steady-state flow models of the valve.

As a first try the simulations were performed on different prototypes under study, all using the same valve body and piston support structure but changing the piston head shape among the following options:

1) Simple plastic hemisphere with rubber sealing;
2) Rubber hemisphere with a slightly flattened shape;
3) Rubber hemisphere with a more tapered and fluid-dynamics shape.

Iterative trial and error process testing the above-mentioned prototypes with a different design, starting from a simpler one up to a more accurate configuration based on the results of the simulations, whose main outcomes (the pressure drops) have been summarized in the following Table 4.2.

CFD Pressure drops [mbar]							
Q [l/min]	Specification values	Valve#1 declared	Valve#1 measured	Valve#1 CFD	CFD proto#1	CFD proto#3	CFD *rev.1*
5	3	n.g.*	20.7	5.6	3.2	3	1.5
10	6	80	27.6	22	12	12	6
15	10	190	30-50 **	47	28	27	13

Table 4.2: Pressure drops results

Table notes:
* Value not given by the manufacturer declaration.
** Variable value due to sensor sensitivity (± 10 mbar) adopted in the measurements.

By availing the results of all the base simulations, it was possible to identify the critical areas and parameters that might have a higher influence on the internal flow to create a new revised version (identified by acronym *rev.1*)
In the model of the new revised prototype the geometry was modified accordingly to improve the fluid circulations in the most critical areas (depicted in Figure 4-3) where the geometry influences the fluid-dynamic behavior of the product:

- Larger flow area by reducing the area of the piston (smaller D_{piston}), nevertheless ensuring the sealing action on the valve seat, leakproof action by the rubber piston head.

- Increase length of the piston's supports to guarantee a higher distance and more flow in the fully-open valve configuration ($L_{support}$) with the aim to increase the space available for the stream to reorganize its path and reduce the turbulence upstream the outlet.

- Smoother path for the flow at the outlet (no recirculation and zero speed), avoiding right angles by modeling fillets and chamfers with a geometry that preserves the function of seat for spring and piston's supports.

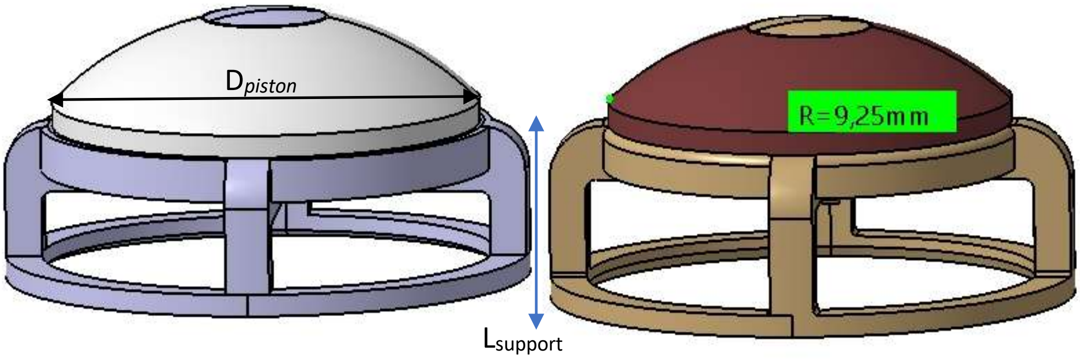

Figure 4-3: Pistons geometry comparison rev1

In the last column of Table 4.2 its performances are compared with the original version:
it was achieved a significant p-drop reduction of about 50% for all the values of flow under study, confirming the crucial role of the modified parameters on the flow.

In the following are reported the complete simulation results and analysis of just the best revised prototype (*rev.1*) that has been chosen among all the possible candidates from the table.
All the pictures reported in this section refer to the outcomes of the simulation in the maximum flow rate configuration (*Q*=15 l/min) since it's the most critical one.

The pressure field, and also the velocity profile in the following analysis, are displayed in a longitudinal section in the center of the valve, far from the piston's support legs since they could obstruct the fluid stream and without considering the impact of the spring.

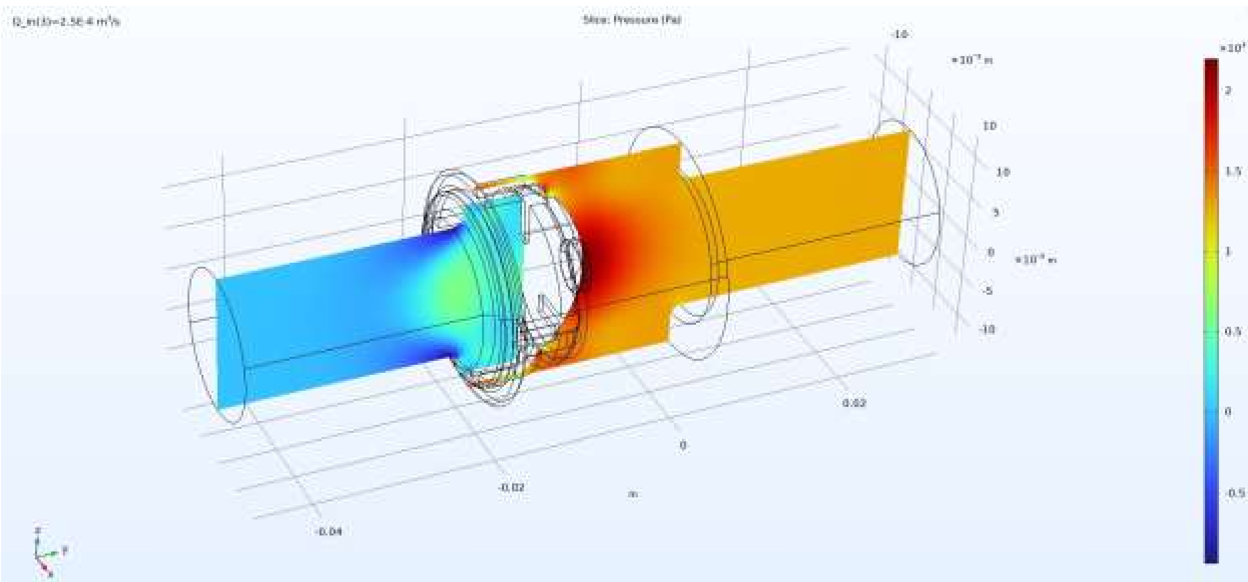

Figure 4-4: Pressure field

Analysis of **pressure**:
Higher pressure levels at the inlet of the valve, since the pressure initially grows up to the cracking pressure level (around few millibars) to open the valve and then maintains the maximum value on the central piston head from where the flux is splitted all around it.
The different design options, such as fluid dynamic shaped piston or simpler one, were tested to compare the results but the outcomes in terms of velocity were very similar in all cases, meaning that the fluid velocity is imposed mainly by the flow area and not by the piston's head shape, since it has a very limited extension.

The pressure level drops where the flow reaches the maximum velocity in lateral restriction areas, between walls and piston, where the velocity profiles suddenly increase its values (related Figure 4-6: Velocity profiles).
In facts, the pressure *p* and velocity *v* of the fluid stream are always strictly related by *Bernoulli's principle*, according to which an increase in speed *v* must be accompanied by a simultaneous decrease in the pressure *p* in order for the sum to add up to the same constant number [12].
Assuming that there is negligible or no change in the height of the fluid so that the potential energy cancels out, the following formula expresses this relation:

Equation 12
$$p + \frac{1}{2}\,\rho\, v^2 = constant$$

Downstream the piston the pressure still decreases at the outlet channel where it reaches almost negligible values close to ambient pressure.

The pressure loss on the valve prototypes was calculated as the difference between the mean inlet and outlet pressures, evaluated as the average value over a surface normal to the flow stream in two fixed points of the valve in any prototype configuration:

- Red reference at the inlet, higher pressure (*p1*);
- Blue reference at the outlet, almost null pressure ($p2 \cong 0$).

This value has to be compliant with the specification's requirements (Table 1.2).
Considering the appropriate units' conversion from Pa to bar, the final **pressure drop** was calculated and plotted as function of the volumetric flow rate, in the working range of interest, in the following Figure 4-5:

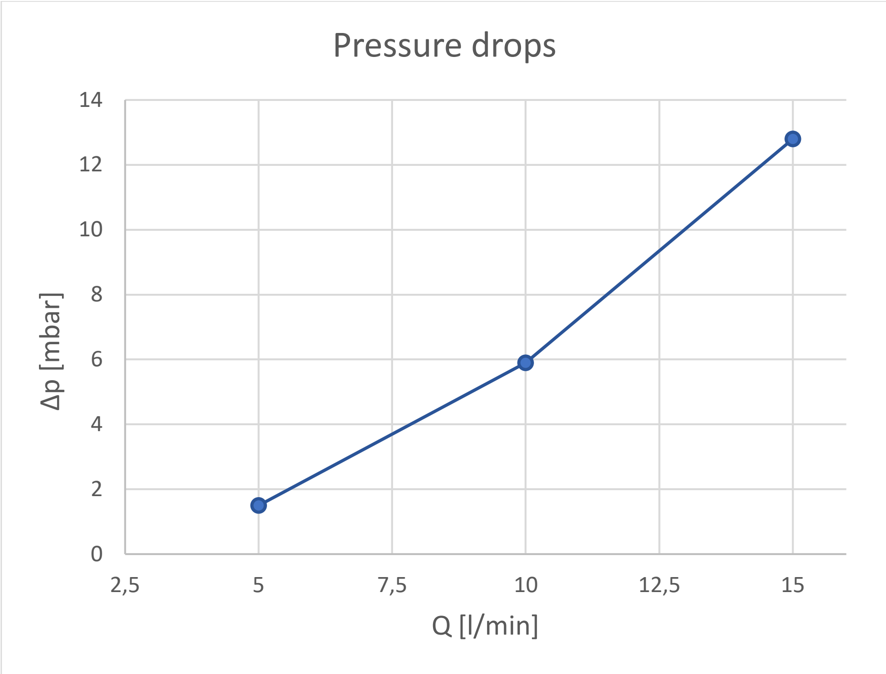

Figure 4-5: Pressure drops as function of volumetric flow rate

The above plot of the simulation's results confirms the theoretical relation, according to which in turbulent regime the pressure drop is proportional to the square of the volume flow rate across a stream section:

Equation 13
$$\Delta p \propto Q^2$$

For that reason, the plot shows a steep increasing trend for values between 10 and 15 l/min (0.17 – 0.25 dm^3/min in the plot) but with values that are in line with the ones imposed by the requirements.
On the contrary the CFD model used seems to underestimate the pressure loss for lower flow values, around 5 l/min (0.08 dm^3/min) because of the initial simplifying hypothesis, in facts the model was simulated in a fully open configuration, neglecting the initial cracking pressure to start the stream and the initial opening motion of the piston against the pre-compression force by the spring, which is not present in this model.

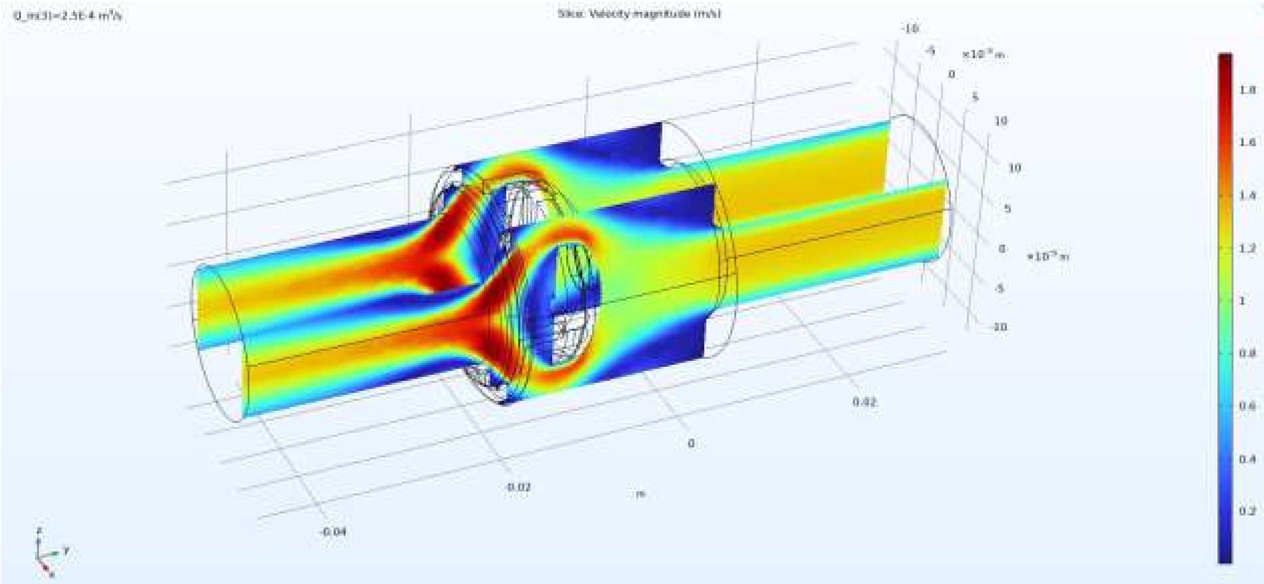

Figure 4-6: Velocity profiles

Analysis of **velocity**:
Max speed in restriction areas where pressure was previously shown to decrease, highlighted by the red color; null velocity values are present in corners, visible blue areas, caused by the recirculatory phenomena of flux (highlighted in next Figure 4-7).
The stream velocity decreases in correspondence of the wall because of friction between coolant and valve boundaries, reaching null values on the no-slip solid boundaries.
According to the outcomes of the simulations the fluid velocity resulted being directly proportional to its volume flow rate, obtaining values respectively around 0.6, 1.2 and 1.8 m/s for increasing Q values.

In a similar plot the flux **streamlines** have been represented to highlight the vortexes and areas of major turbulence, such as the restriction of the flow between the plunger's head and valve body, or the area downstream the piston head where some recirculation of the flow takes place before reaching the valve outlet (Figure 4-7) .

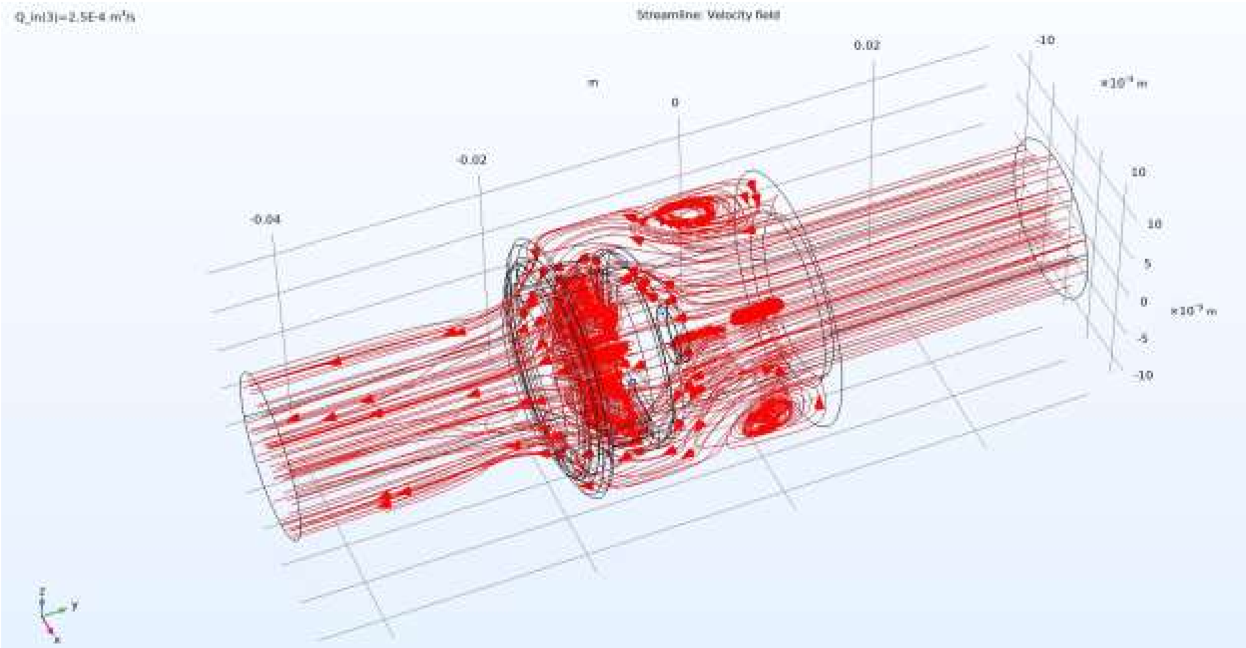

Figure 4-7: Flow streamlines visualization

Recirculation of fluid stream seems to be mainly present in steep change of flow area between inlet and valve body, but since this phenomenon is present far from restriction and outlet, it should have small or no influence on the pressure drops performances of the product.
In addition, at increasing values of flow rate the recirculation was shown to be reduced, as the liquids energy and speed are higher and it shows the tendency to proceed in a straight direction until it’s deviated by the piston head.

4.5 Initial model assessment

Some improvements of the model were performed through an iterative process of simulations and correlation with physical bench tests on some functional prototypes.

Several experimental measurements (see description in benchmarking activity chapter 2) on 3D printed prototypes were conducted to obtain a practical indication about the influence of the piston's **material** and **shape** on the pressure drop they cause in the same valve body (iso-body tests).
The aim of this activity was to compare different materials for the piston head, such as plastic, rubber and silicon, to analyze more in detail their performances and establish a tradeoff between backflow sealing and pressure loss to respect all the technical specifications for the final product.

In particular the following comparison is carried out testing rubber and silicon pistons with different shapes, same used in the CFD simulations (chapter 4.4):

- Shape #1, simple hemisphere
- Shape #2, tapered and fluid-dynamics shape.

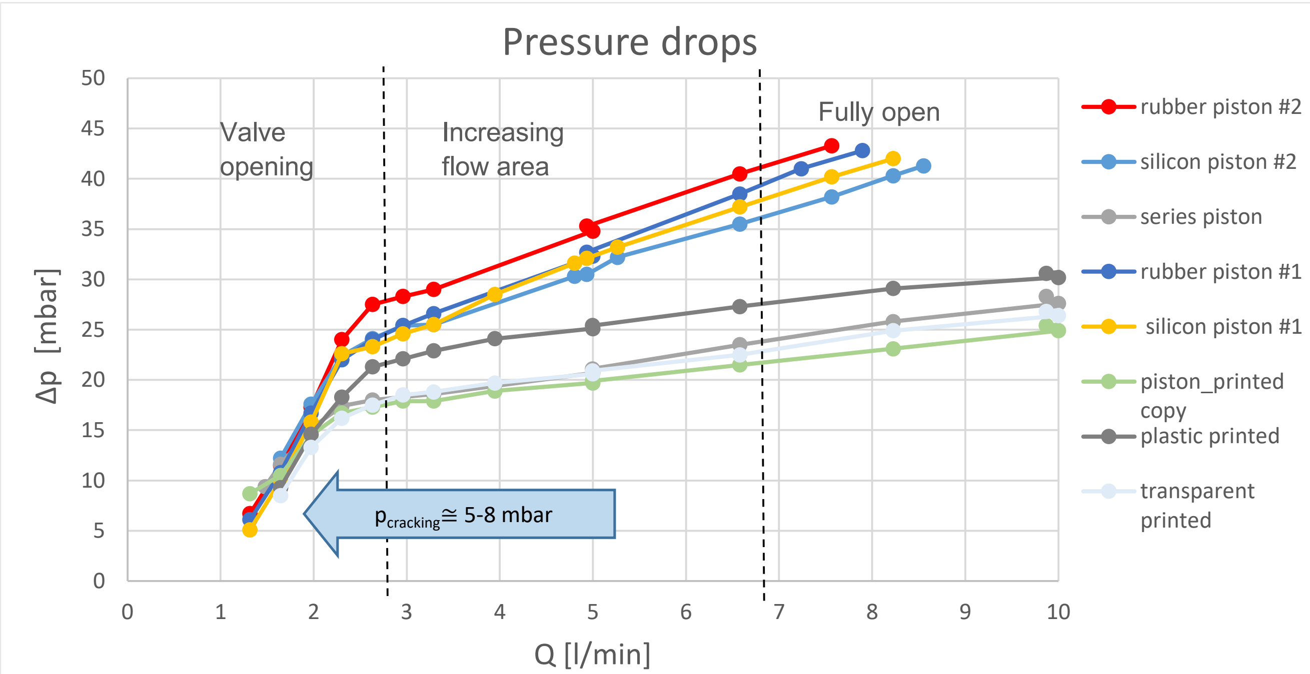

Figure 4-8: Experimental results comparison

The experimental results of pressure losses as function of the flow rate were reported above and show this particular behavior:

- at low flow values the delta pressure between inlet and outlet remains positive and constant until the cracking value is reached, so that the valve opening starts; immediately after the valve opening the pressure loss increases steeply with the volume flow rate since the flow area is still very limited;
  This part of the curves' slope is mainly influenced by the spring stiffness and pre-compression, main reason why the prototypes (4 upper curves) show a different trend with

a higher slope because of a small difference in piston geometry and spring pre-compression.

- at medium-low flows the piston is pushed back inside the valve body, with a transient and dynamic motion, causing a large increase of the flow area and consequently a more linear pressure drop. The curve slope depends on the flow area and piston volume inside the valve body.

- at higher flow values the piston reaches the fully-open configuration and the delta pressure tends to become more stable and slowly increasing, since the static configuration has been reached and the losses depend only on the piston shape and geometry that influence the obstructing action at the outlet.

As an outcome of the activity it was found out that in all the cases the rubber material causes more pressure losses than the silicon one; this could be due to the higher roughness and friction factor of the rubber.
Instead the more complex piston's shape #2 didn't show significant benefits if compared to the experimental results coming from the simpler piston with shape #1; this was confirmed also by the CFD simulations that gave very similar results in terms of pressure losses with both the shapes (see proto#1 and proto#3 in Table 4.2).
On the contrary the higher values of pressure loss from the designed prototypes were mainly due to their volume that is larger than the series piston's one to guarantee the sealing action but at the same time causing more restriction to the fluid stream inside the valve body; consequently, the geometry of the flow area was confirmed to be the main cause of pressure losses.

In conclusion, the results of the initial simulations coming from our CFD model (reported in Table 4.2) seemed to underestimate the pressure drops values related to the minimum flow simulation ($Q1$ = 5l/min), in facts all resulted being too low with respect to the measured values…
A first reason for a slight difference between the simulation results and bench tests may be due to uncertainties and errors during the execution of the latter but the main reason should be attributed to the model that still needs some tuning, which is the main argument of the next chapter of this thesis work (Chapter 5).

5 Tuning of CFD model based on experimentation results

The comparison between the physically measured pressure drops and CFD simulations data can provide insights into the accuracy and correlation of the model with the real-life behavior.
To perform this process a CAD model of the valve #1 from the benchmarking activity was created, starting from the physical measurements on the physical body. Then, after discretizing the fluid control volume, it was possible to get some CFD results regarding its pressure loss.
In this way a comparison between the initial fluid-dynamic model and the physical counterpart results is plotted in Figure 5-1.

Figure 5-1: Models p-drops comparison

Correlation of results:

The plots shown above follow a similar trend but with an initial offset, in facts the results must consider not negligible pressure loss in the physical test setup due to the additional length of the connections and instrumentations needed. In the volumetric flow rate ranges between 5 and 10 l/min similar trends and slopes have been obtained in both the cases, but still influenced by the initial offset.

Indeed, our CFD model seems to underestimate the pressure loss for low flow values, in which *Q1* identifies the 5 l/min configuration, since the model is simulated in a fully open configuration, neglecting the initial cracking pressure to start the flow and the initial opening of the piston due to the closing force by the spring, reason why a tuning process was carried out.

A series of CFD simulations were performed on the newly designed prototype under test (valve *rev.1*) in different transient opening positions, evaluated by force balance between the liquid pressure on piston and the opposite spring force, expressed by Equation 14:

Equation 14

$$p_1 * A = k * \Delta x$$

Where:
p_1 is the average value of pressure at the valve inlet [mbar];
A is the piston cross section on which it acts [mm^2];
k is the designed spring rate [N/mm];
Δx is the total deformation of the spring at the equilibrium position, also considering the pre-deformation, from the spring free length L_0 , in the closed-piston configuration.

Equation 15

$$\Delta x = L_0 - L$$

This procedure required an iterative approach, starting from the almost closed valve configuration (simulated with 1mm opening) in which *p1* and *A* are the values measured at the inlet of the valve. Instead, proceeding with the iterations, in an intermediate opening valve state the fluid pressure *p1*, that acts on the entire plunger frontal cross section during the stream, must be measured as the average pressure value inside the central body upstream of the piston's head.
The *bisection method* was applied, repeating the CFD simulations in an iterative way to measure the pressure value *p1* in displacement configurations obtained bisecting the interval of the *x* values from the previous simulations and selecting the subinterval in which the calculated spring and pressure forces have closer values.
Repeating this method different times (with 14, 6, 3 and 2 mm of piston displacement) an approximate convergence was reached, therefore identifying a possible equilibrium position for the simulations at the minimum volume flow rate value imposed (*Q1*).

A qualitative plot of the forces after 6 iterations is here reported in Figure 5-2:

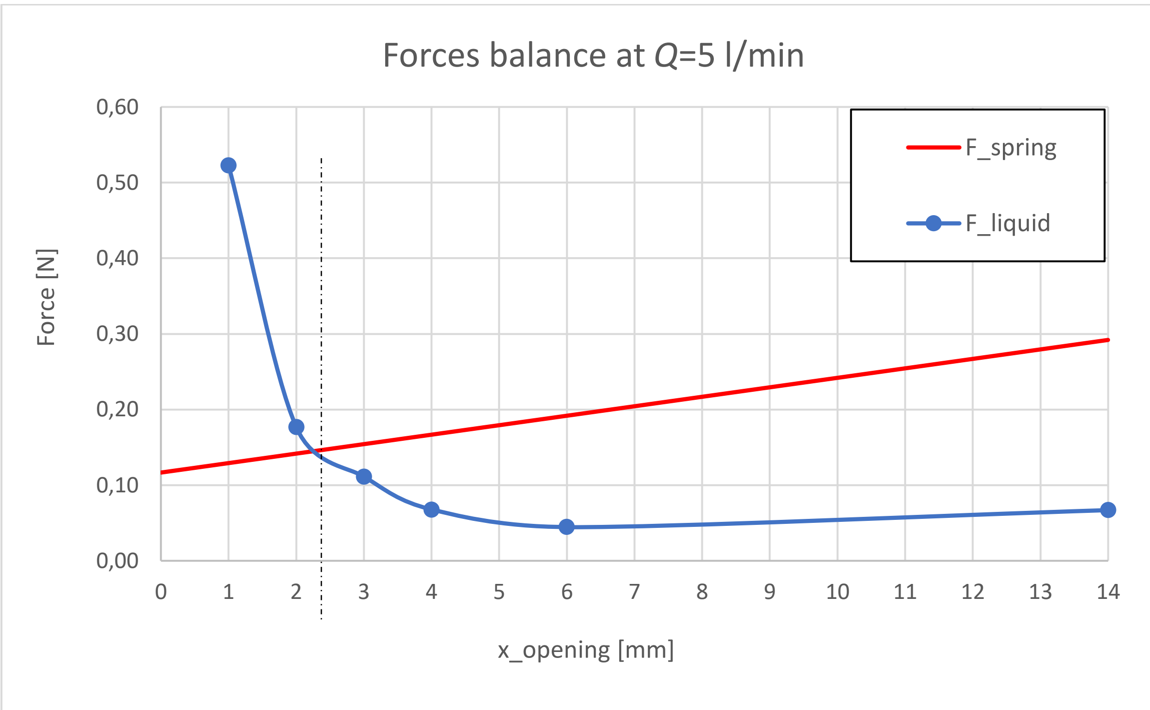

Figure 5-2: Force balance at equilibrium

- the **spring** force varies linearly with the spring displacement, starting from an initial offset due to the preload that represents the cracking force to start moving the piston and a low-inclined slope corresponding to the very limited value of the spring stiffness, designed to have a value around 0.0125 N/mm.

- the **liquid** force instead decreases with the opening position in a not linear way, interpolating the 6 points coming from the CFD measurements and calculations, showing a very steep decrease in value after the first very few millimeters of opening, instead after an initial stroke of around 3-4 mm its value settles down to an almost constant value, meaning that from that opening point on the flux inside the valve gets more stable since the flow area of the body is constant.

In the same way the inlet pressure value was plotted as function of the opening position (x) to obtain a good approximating graphical outline that could be interpolated to obtain the inlet pressure value ($p1$) corresponding to any position of the piston, within the range of deformation represented by the physical boundaries of the valve.
This resulting plot (Figure 5-3) was obtained interpolating the 6 values of inlet pressure obtained from the model CFD simulations in the corresponding opening positions:

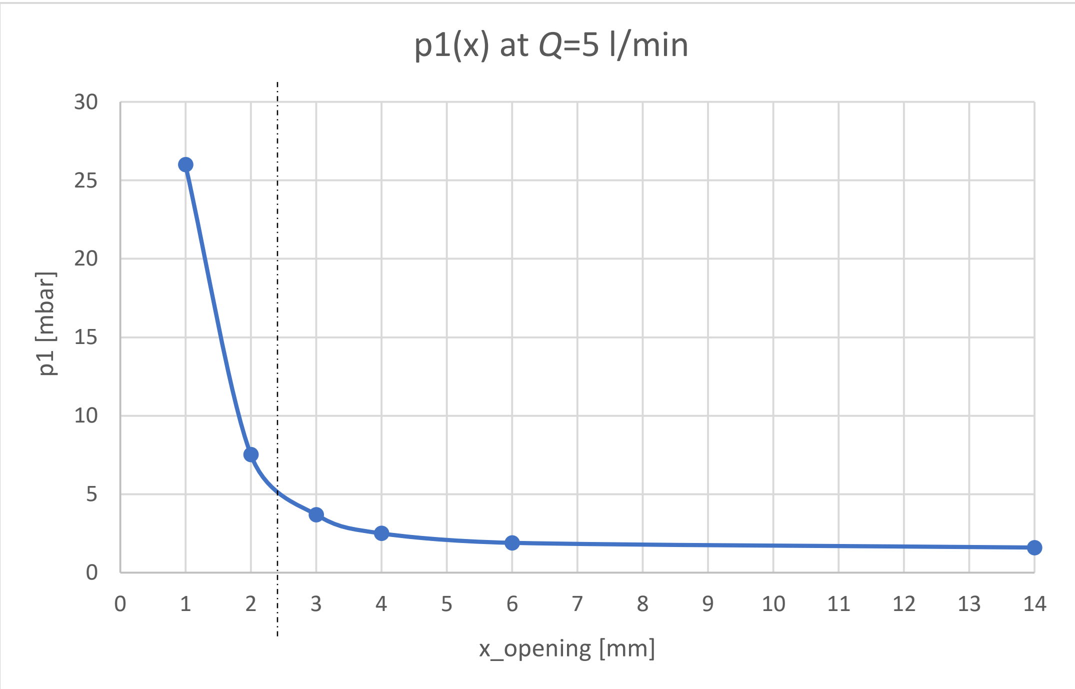

Figure 5-3: Inlet pressure p1 at equilibrium opening position

The inlet pressure level shows a steep decrease after the first few millimeters of piston opening, because of the increasing flow area inside the valve body, and then it tends to stabilize around a more constant value until the fully open configuration where the pressure drop results being minimum.
The next step was the creation of one model in the final equilibrium configuration to be tested, just in the minimum flow rate condition ($Q1$=5 l/min), and repeat the simulation for the prototype under study.
An example of the fluid domain cross section in equilibrium configuration is depicted below in Figure 5-4.

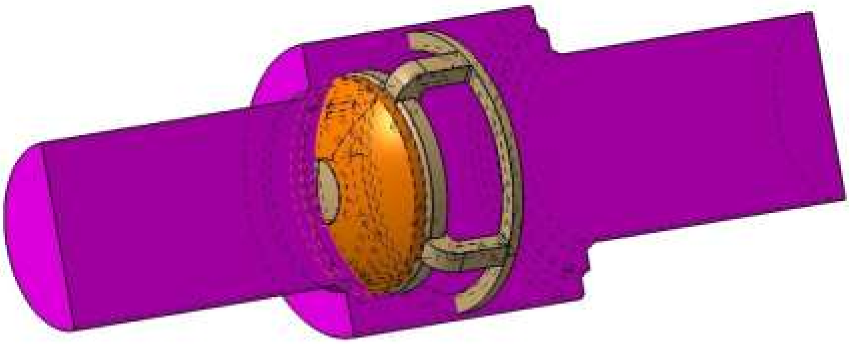

Figure 5-4: Fluid domain control volume, equilibrium configuration

From this former study the equilibrium condition was estimated being between 2 and 3 mm of opening , highlighted by the vertical dotted line in Figure 5-2 and Figure 5-3.
To confirm the approximation a final CFD simulation was performed on a model in this equilibrium configuration under study, with 2.5mm of valve opening. The graphical results are reported in the following plots of Figure 5-5 and Figure 5-6 :

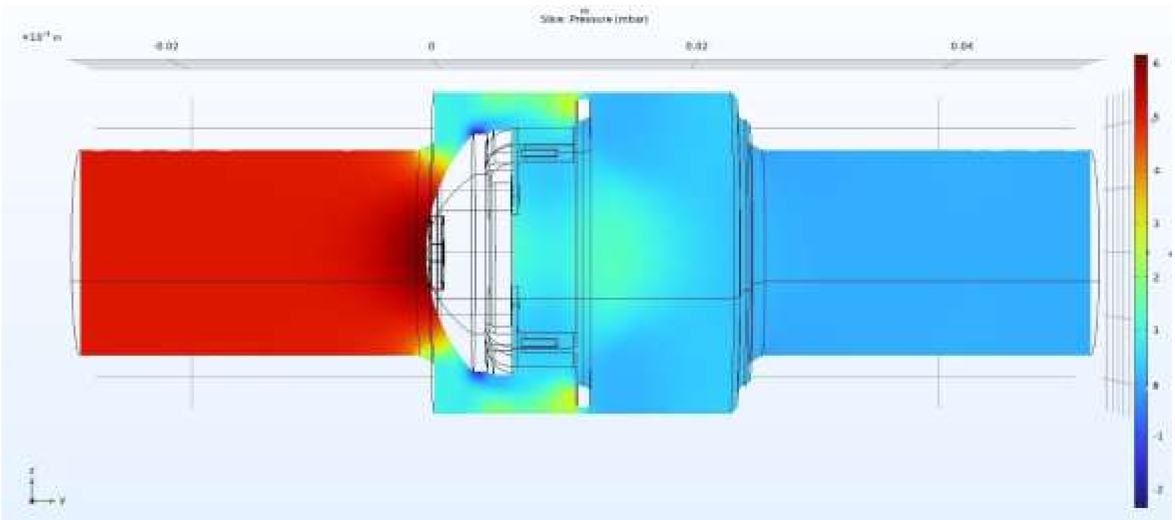

Figure 5-5: Pressure field in equilibrium configuration

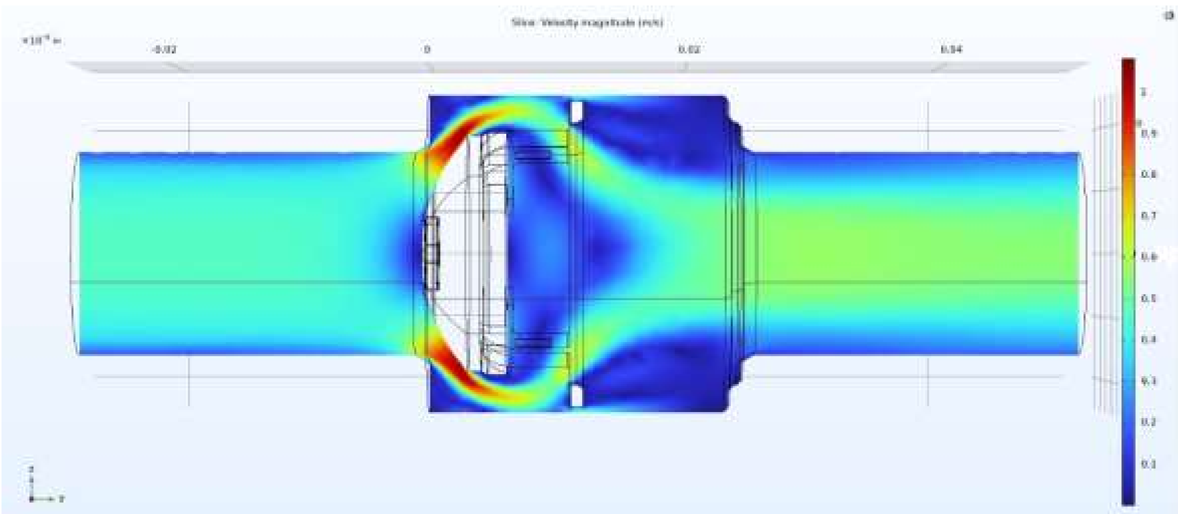

Figure 5-6: Velocity field in equilibrium configuration

Pressure and velocity field analysis:
As expected from this simulation with a low valve opening, the critical behavior takes place in the restricted flow area.
In Figure 5-5 it's clearly visible the maximum pressure level at valve inlet because of the low opening of the piston, almost ambient pressure at the outlet; in conclusion the simulated pressure drop was evaluated to be approximately **5 mbar**.
The other useful plot, Figure 5-6, shows the maximum speed between piston head and inlet channel, but still low value (max 1 m/s) since the flow rate under study is at the minimum value. Minimum flow velocity, almost null in magnitude, downstream the piston support and in the body's corners where the recirculation phenomena take place.

This simulation result turned out being higher than the one obtained in the fully-open valve configuration for the same flow conditions and valve prototype (*rev.1)*, as expected because of the initial restricted flow area, clearly shown in the zoom of Figure 5-7, in which the velocity field of the flow is represented by the red arrows and the pressure loss takes place on the circular sector on the piston head where the flow speed increases.

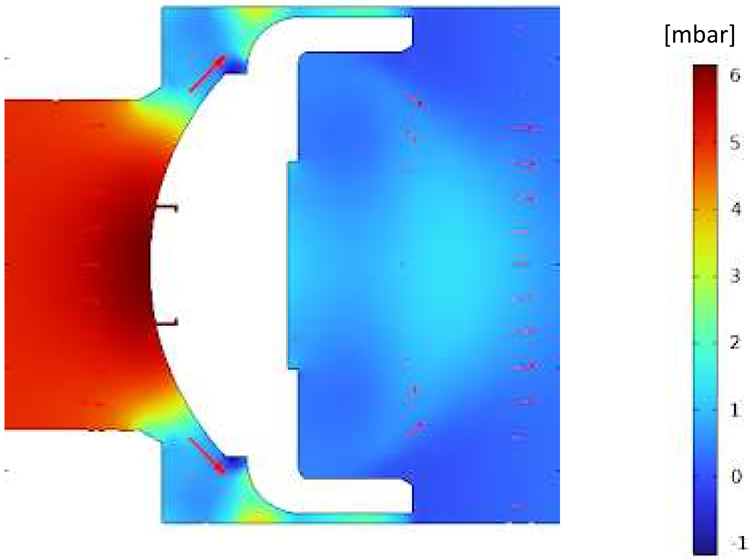

Figure 5-7: Zoom on restricted flow area of the equilibrium configuration

Nevertheless, this final Δp value results being almost in line with the specification limit and comparable, or even lower, than those of the competitor tested with the same CFD model.
These main results are summarized in Table 5.1.

CFD Pressure drops [mbar]					
Q [l/min]	Specification values	Competitor #1	Initial proto	Proto *rev.1*	Proto *rev.1* tuned
5	3	5.6	3.2	1.5	**5**
10	6	22	12	6	5.9
15	10	47	28	13	12.8

Table 5.1: Pressure drop final comparison

After the determination of the Q-Δp characteristic for the final prototype of the valve, it is useful to estimate its discharge coefficient $\boldsymbol{C_d}$, defined as the ratio of the flow rate at the discharge end of the flow restriction to that of an ideal flow which expands the same working fluid across the same pressure drop of the restriction.
Its value can be obtained by reversing the formula that links pressure difference and volume flow rate for an orifice, because the only unknown parameter is the discharge coefficient itself.

Equation 16

$$C_d = \frac{Q}{S\sqrt{\frac{2\Delta p}{\rho}}}$$

Q is the volume flow rate of fluid through the restriction, imposed for each simulation configuration [l/min];
Δp is the pressure drop across the restriction, evaluated by the numerical simulation [mbar];
S is the flow area, whose restriction depends on the opening configuration of the piston [mm^2]
ρ is the fluid density, imposed by the technical coolant requirements

Therefore, this a-dimensional value is not constant but it changes for each configuration that has been tested:

- for Q1 the flow area considers the equilibrium configuration with the restricted flow area, whose value is estimated from the technical drawing,
- the higher flows are related to a fully open valve with a larger flow area.

The calculations have been made accordingly for each case, performing the necessary conversion for the units of measure [*m, Pa, s*] and so on; the results are here summarized in

Configuration	Q [l/min]	Δp [mbar]	$\boldsymbol{C_d}$ [-]
1	5	5	0,90
2	10	6	0,69
3	15	13	0,71

Table 5.2: Estimated values of discharge coefficient foe each working configuration

Theoretical behavior of product from calculations results:
cracking pressure to start opening the valve estimated being around 6 mbar; then the pressure drop level decreases slightly with the progressive displacement of the piston; afterwards the CFD results showed that the equilibrium position is reached, around an opening of 2.5 mm in correspondence of the 5 mbar pressure drop for the flow rate of 5 l/min,

For the moment it should be considered that in this process some errors could be present since the CFD model of the valve is still subjected to some simplifying assumptions.

Lastly, the ultimate goal of this chapter was to create a reliable and useful model of the product for future industrialization, therefore once the CFD model will be validated, it could be trusted to provide reliable predictions, which significantly reduces the need for experimental trials, representing a save in time and financial resources for the company.

6 Manufacturing of first functional prototypes

After the material and assembly process selection (see dedicated chapter 2) a functional prototype composed of valve body, outlet flange, piston support was obtained through 3D printing choosing a resin whose mechanical properties are as similar as possible to the ones of *PA66,* even though some material discrepancies are still present.
At the same time the piston head was printed with a softer silicone resin to guarantee the sealing action of the piston head against its seat.

In addiction a spring prototype was supposed to be manufactured by winding an harmonic steel coil, with the proper diameter, around a die designed to obtained the desired spring geometry and mechanical properties, the stiffness firstly. This complication is due to the very low stiffness and not standard dimensions of the spring for this specific application, making unfeasible the choice of a similar product from a supplier catalogue.
Unfortunately, this manual manufacturing operation wasn't feasible because of the memory properties of the harmonic steel that tends to return to its undeformed shape, making it impossible to wind it properly to obtain the desired spring shape.

During the clip interference assembly a radial O-ring, properly calculated and selected from a standard catalogue, must be installed to guarantee the sealing action for a leak-proof connection between the two main bodies composing the valve.

Figure 6-1: Parts composing the new functional prototype

Test on new functional prototype for CFD model tuning and guarantee the respect of design specifications and requirements, comparing performances with benchmarking results.

At this point the performances of the new functional prototype must be examined through the same tests carried out during the benchmarking activities, detailed description in chapter 2.

7 Definition and implementation of a test plan for Concept Validation

In order to validate and make quantitative comparisons between new designed prototype and products from competitors tested during benchmarking, it was necessary to repeat the most important tests conducted and described in details during these activities (see dedicated chapter 2) A series of experimental tests have been conducted with the objective of evaluating the accuracy and precision of the CFD model's results in terms of pressure drops but also compare the performances of the functional prototype, due to the new design, with the products examined during the benchmarking.
This approach serves not only to validate the functionality of the check valve, but also to facilitate a detailed comparison between the main technical requirements of the part and its actual performances.

7.1 Pressure drops

The main test is linked to the evaluation of the pressure drops experimentally, through the water column height methodology (described in chapter 2.1).
A challenge for the experiments was due to the absence of a spring in the prototype, consequently this test was conducted in two different ways:

- using a piston in the fully open configuration for the higher levels of flow (Q =10 and 15 l/min) to replicate the layout of the CFD model in these conditions;
- utilizing a modified piston with elongated supports to replicate the opening configuration corresponding to the equilibrium condition of the valve for the lowest flow value (around 3 mm for $Q1$= 5 l/min), as obtained from the CFD model tuning process.

For this final analysis the prescribed liquid coolant (water and glycol 50% mix) was used, adopting all the necessary safety precautions and personal protective devices, in order to guarantee a complete accordance between CFD and physical simulations working fluid.
All the experiment-based results are plotted in the following Figure 7-1:

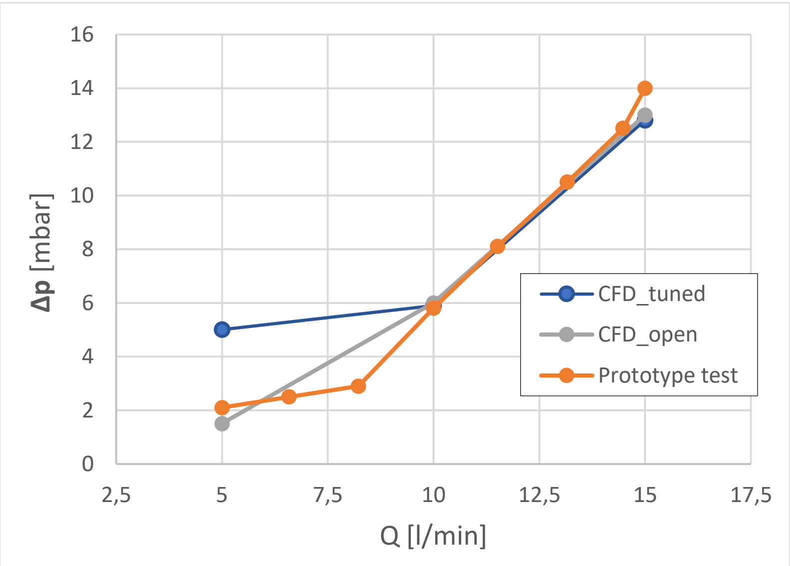

Figure 7-1: CFD and experimental pressure drops comparison

From the previous plot it's possible to compare the test results with the expected outcomes from preliminary CFD models calculations:

- very good approximation at high flow values (after 10 l/min); in this range the model resulted being well validated by the experimental results.
- at minimum flow the experimental results are closer to the ones from the base CFD model, (simulating the fully open valve) with respect to the tuned model that simulates the valve with the piston in the equilibrium intermediate position. This could be due to a small dimensional discrepancy between the printed piston positioning, probably vibrating and moving inside the valve, and its fixed position in the tuned CFD model.

In the end the prototype behavior in terms of pressure loss is compared with the competitors' results on the same bench test. Their performances are plotted in Figure 7-2:

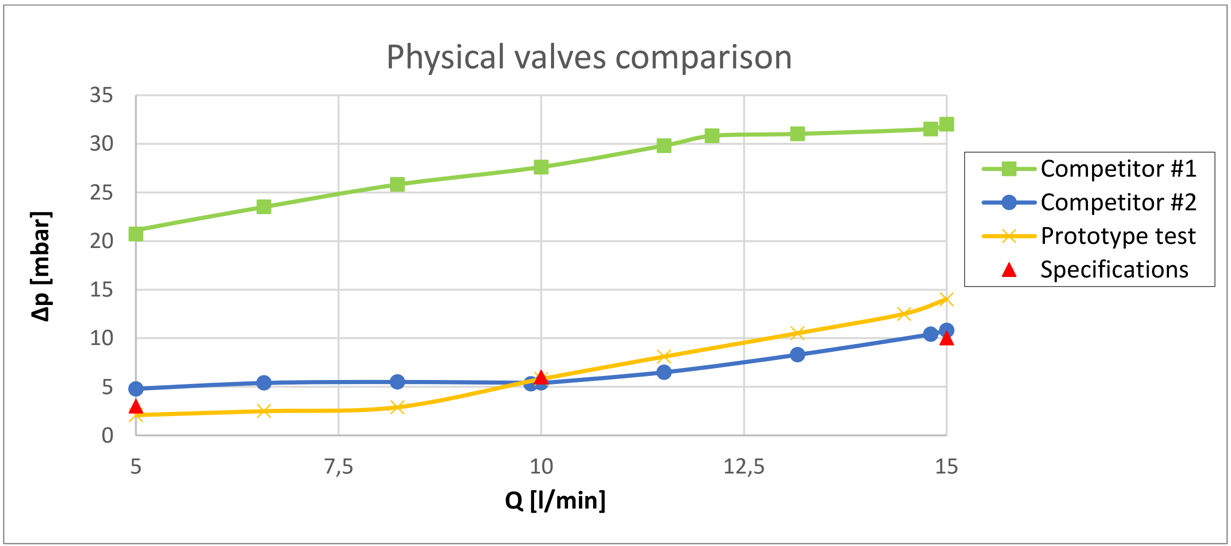

Figure 7-2: Experimental results: physical valves comparison

These bench test results of Figure7.2 highlight a good behavior of the physical prototype, comparable with valve from competitor #2 that also resulted the one being closer to the specifications values, just discretized in 3 flow values and highlighted by the red triangles on the plot. In facts the bench test showed pressure drops values slightly larger than the required ones just in the higher flow range of interest (10-15 l/min) but still acceptable from a functional point of view.

7.2 Cracking pressure

This value can be computed using Equation 8 (see dedicated chapter 2.6) that considers the force balance between the spring force and the cracking pressure by the liquid to start the opening of the plunger.
The spring, subjected to the designed pre-deformation, exerts a force F_{spring} counterbalanced by the liquid pressure on the circular inlet surface, determined knowing the inlet diameter $D_{in.}$ of the prototype.
All the results are here summarized in Table 7.1:

D_{in} [mm]	16
S [mm^2]	201
F_{spring} [N]	0.12
$p_{cracking}$ [mbar]	**5.8**

Table 7.1: Cracking pressure evaluation

The resulting value is comparable with the competitor's valve#1.

7.3 Overall characteristics

At last, the prototype's characteristics have been studied to respect both the functional specifications imposed at the beginning of the thesis work (chapter 1.2) but also the general requirements for this kind of products, explained more in details in chapter 1.1.

First of all, the dimensional constraints for the product have been respected, in terms of reduced footprint on the cooling system:

- valve length limited to 79mm (about 12% less than tested ones from the competitors);
- maximum body diameter in line with competitors' ones, even if the clip assembly method requires more external spacing;
- estimated total mass around 19 grams (30% to 10% less with respect to what measured in chapter 2.8)

Nevertheless, during this process of concept validation it was not possible to carry out all the tests performed on the competitors' valves during the benchmarking, discussed in the benchmarking chapter 2, for a series of reasons:

- Absence of a physical spring for bypass flow test;
- Discrepancy of prototype's 3D printed material from actual mass-production product, causing some issues during the clip assembly; a bursting pressure test on the proto would not be representative.

In conclusion, the overall objective of these final experiments was to quantify the discrepancy between the intended and actual behavior of the unidirectional valve prototype under study.
After all it's possible to confirm that the product's performances are in line with its theoretical ones expected from the design, thus the validation process could be considered satisfactory.

8 Conclusions

The aim of the thesis project was to research, design and develop a non-return valve for automotive cooling systems in collaboration with "*RAICAM DRIVELINE srl*".

This process was a comprehensive study including many different activities: physical bench tests on existing products, preliminary CAD models creation and drawing of the new valve, FEM analysis on the clip assembly and material, CFD simulations of the flow, subsequent tuning and validation of the prototype.
Each of these steps gave, in an iterative way, some important results related to the performances, geometry, assembly design and compliance with technical requirements of the final prototype in development.

Some critical aspects were linked to the design process: modeling of new components respecting technical constraints and tolerances for the product manufacturing and assembly. In particular this operation followed an iterative procedure to understand the main parameters affecting the performances of all the components composing the valve in terms of geometry, flow area, spring stiffness, piston design and so on.
Other challenges were encountered, such as the development and tuning of an accurate CFD model to simulate the pressure drops through the valve in a satisfactory way but maintaining an acceptable computational power and time.

A final comparison between experimental and numerical simulations results of the functional prototype lead to a validation of the design and numerical model, in facts the test gave positive outcomes, in line with the expectations and the technical requirements.

In conclusion this work can be considered as a starting point for a further analysis, design investigation and testing on series produced unidirectional valves. Furthermore, it will be necessary a deeper tuning and validation of CFD valve prototype in order to get a completely reliable model for future development in other similar applications.

Appendix

A0_Program listings

IntelliMESUR® (load cell software)
CATIA V5 (CAD software)
Solidworks (CAD and FEM analysis software)
COMSOL Multiphysics (CFD software)

A1_Pump characterization

Performed by *Raicam* engineers during the installation of the cooling test bench.

This operation was achieved by measuring the output average flow rate circulated by the pump at some discrete input values of pump's power, imposed through the control wheel scale a-dimensional number. This test was replicated more times, to ensure the repeatability of the measures, and the average value of all the measurements was used for the flow rate characterization as function of the value on the wheel controller (Figure A1.1) and obtain the related plot, depicted in figure A1.2, whose final equation resulted being:

$$Q = 3{,}2861 * \text{value of bench controller [l/min]}$$

In particular the Q values of 5 - 10 and 15 l/min were highlighted since are the most useful reference values imposed by the standards and used for testing.

Figure A1.1: Bench controller

The final coefficient of determination (R^2) declared is extremely close to 1, meaning that the outcomes are well replicated by the model used.

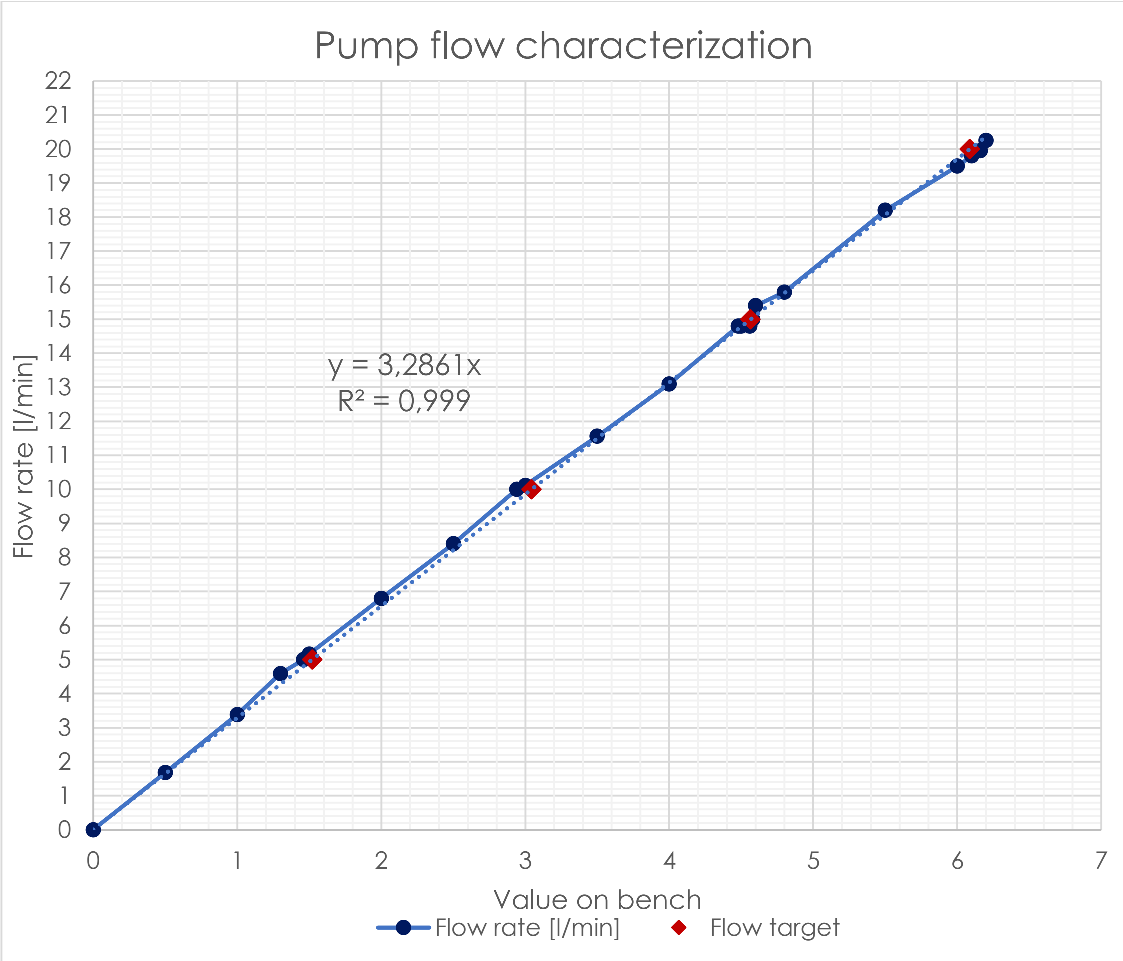

Figure A1.2: Pump flow characterization

A2_Technical drawings

All the following technical drawings represent the prototype 3D components and final assembly designed in the dedicated section using the *“CATIA V5”* CAD software.

In the drawings the most sensitive results, such as dimensional and geometrical tolerances, dimensioning coming from assembly calculations and precise values of most important functional outcomes are not shown numerically in this thesis work for corporate confidentiality reasons.

The following 7 drawings (prototype state) are reported in the following section:

1. Check valve body
2. Check valve outlet flange
3. Piston support
4. Piston head
5. Spring
6. O-ring
7. Product final assembly

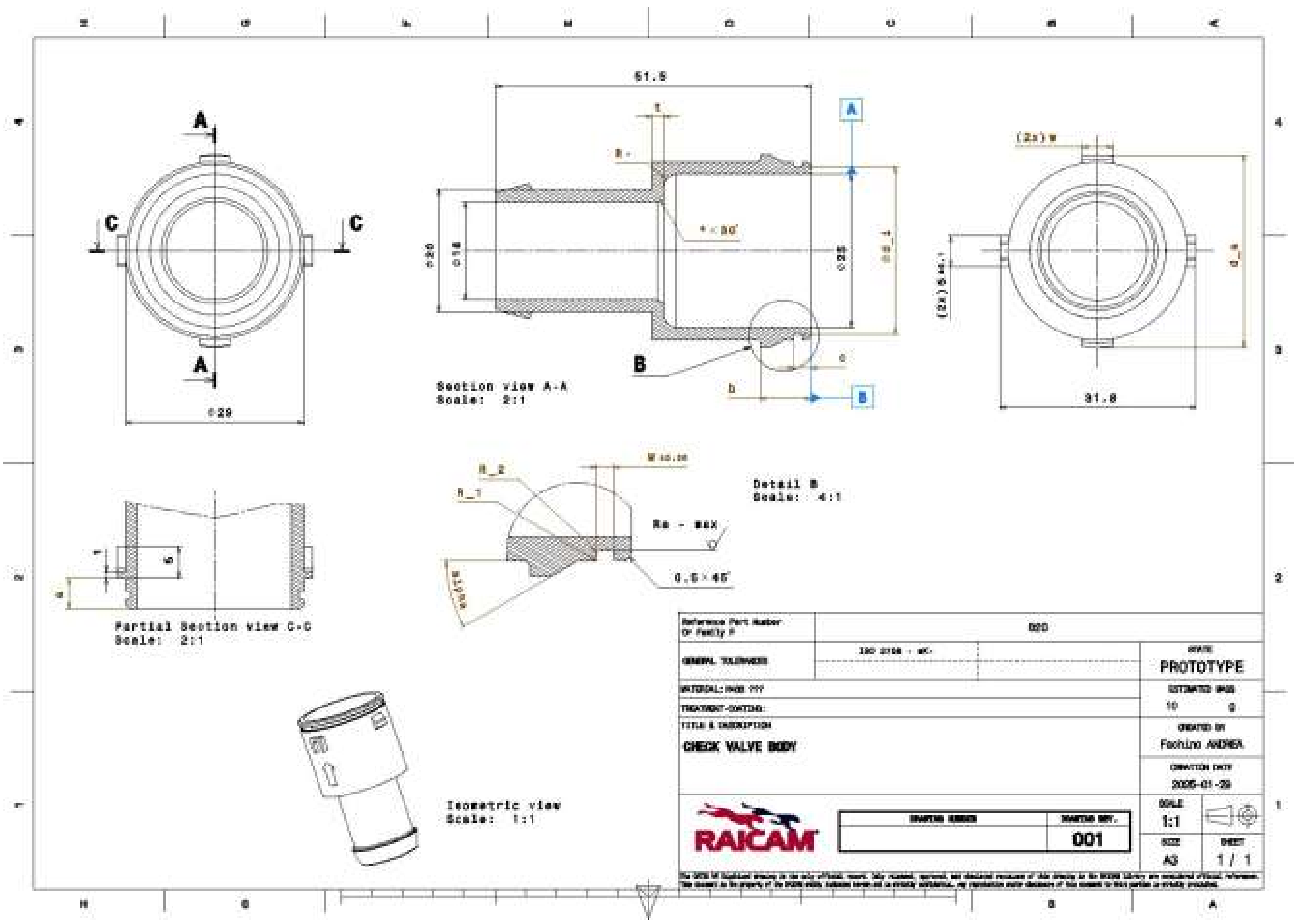

Figure A2.1: Check valve body _ technical drawing

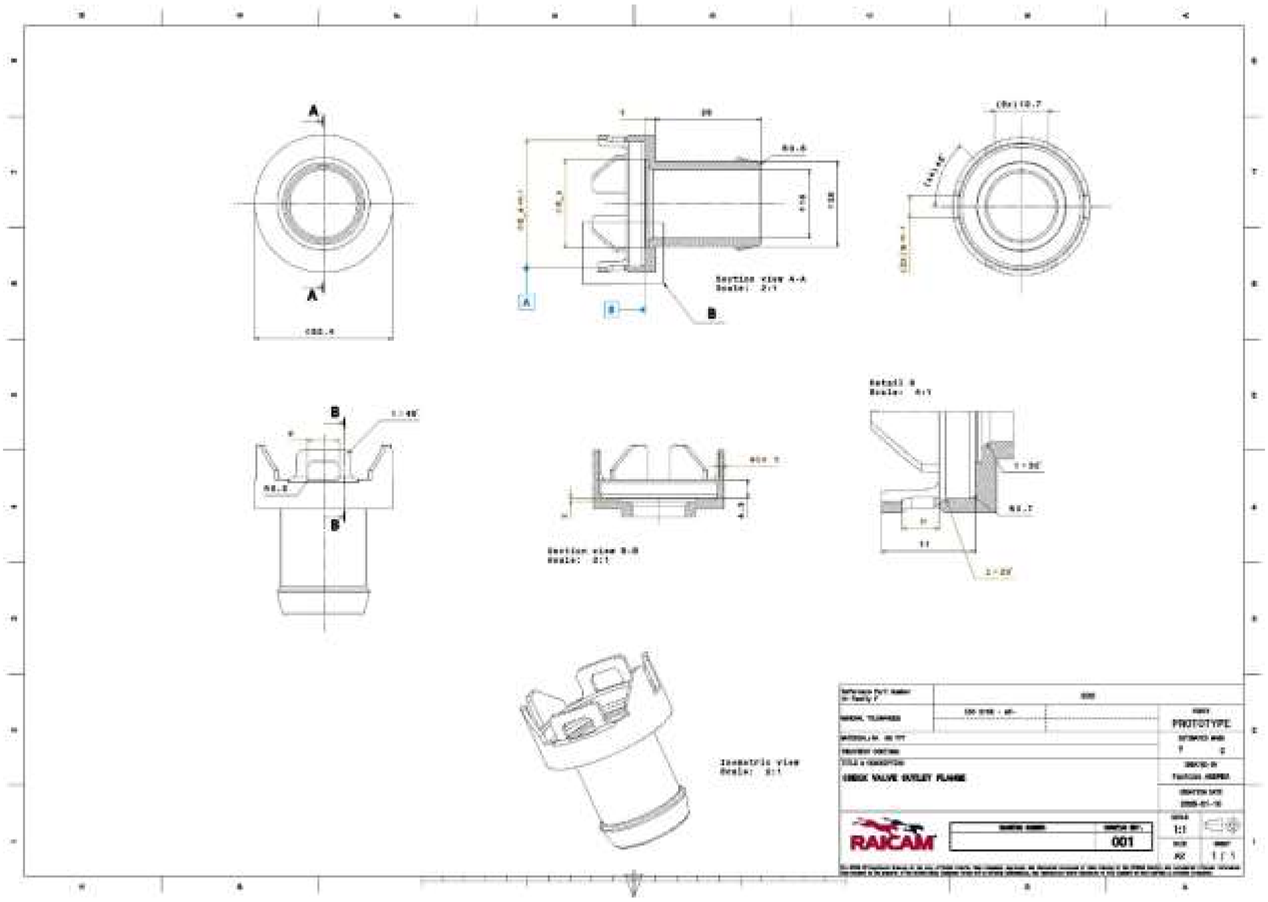

Figure A2.2: Check valve outlet flange_ technical drawing

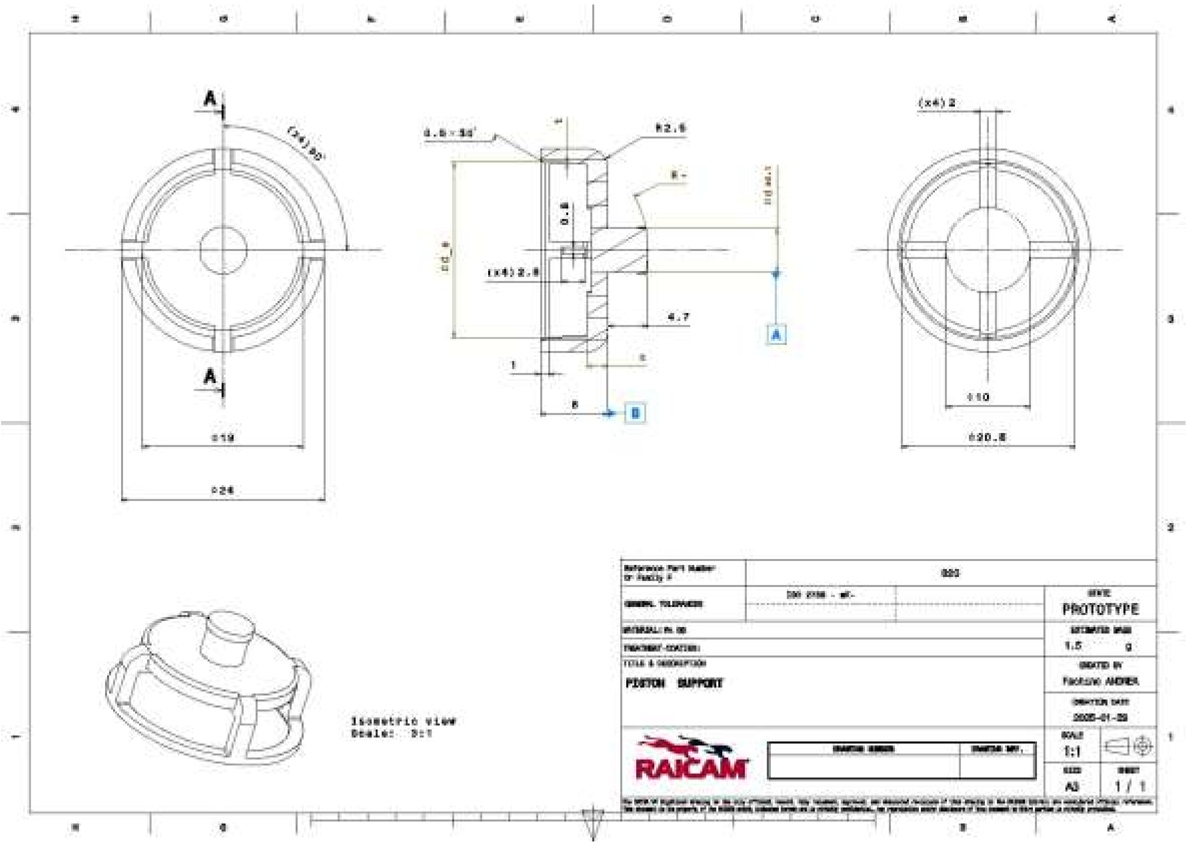

Figure A2.3: Piston support_ technical drawing

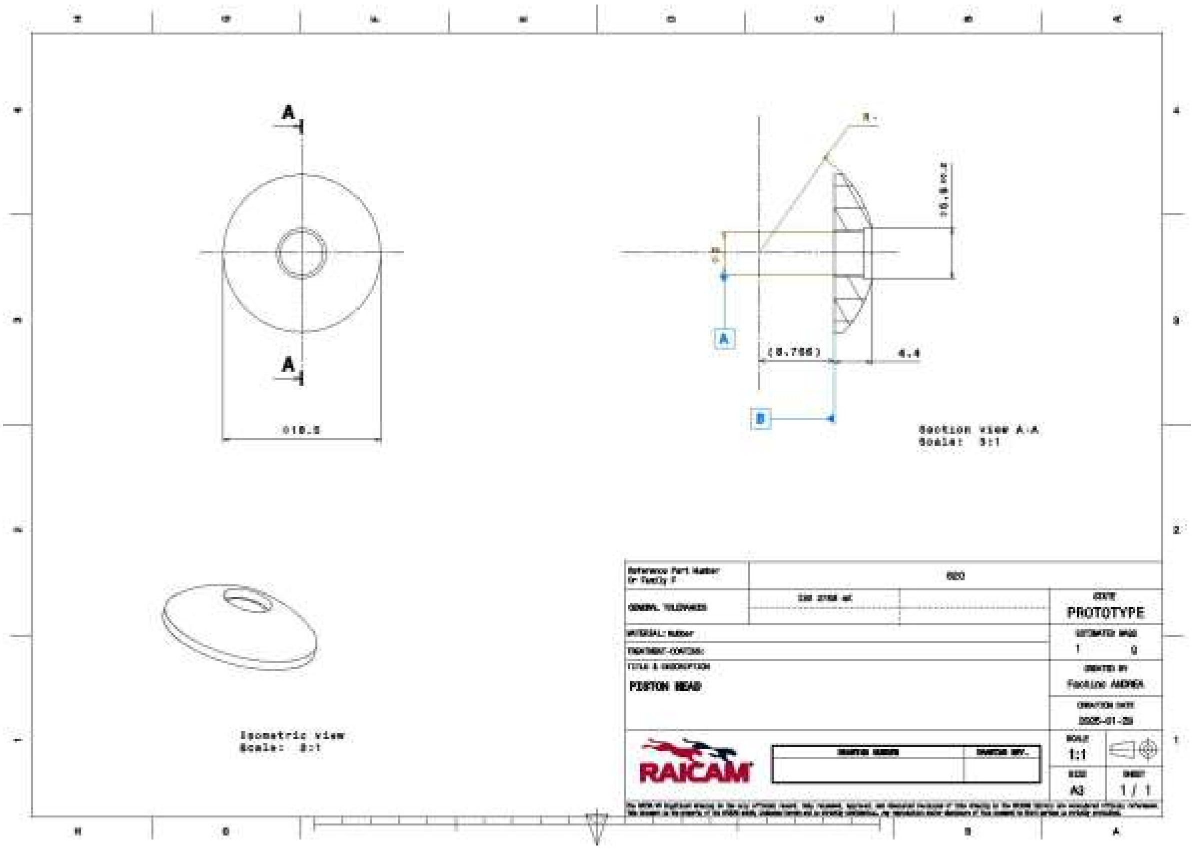

Figure A2.4: Piston head_ technical drawing

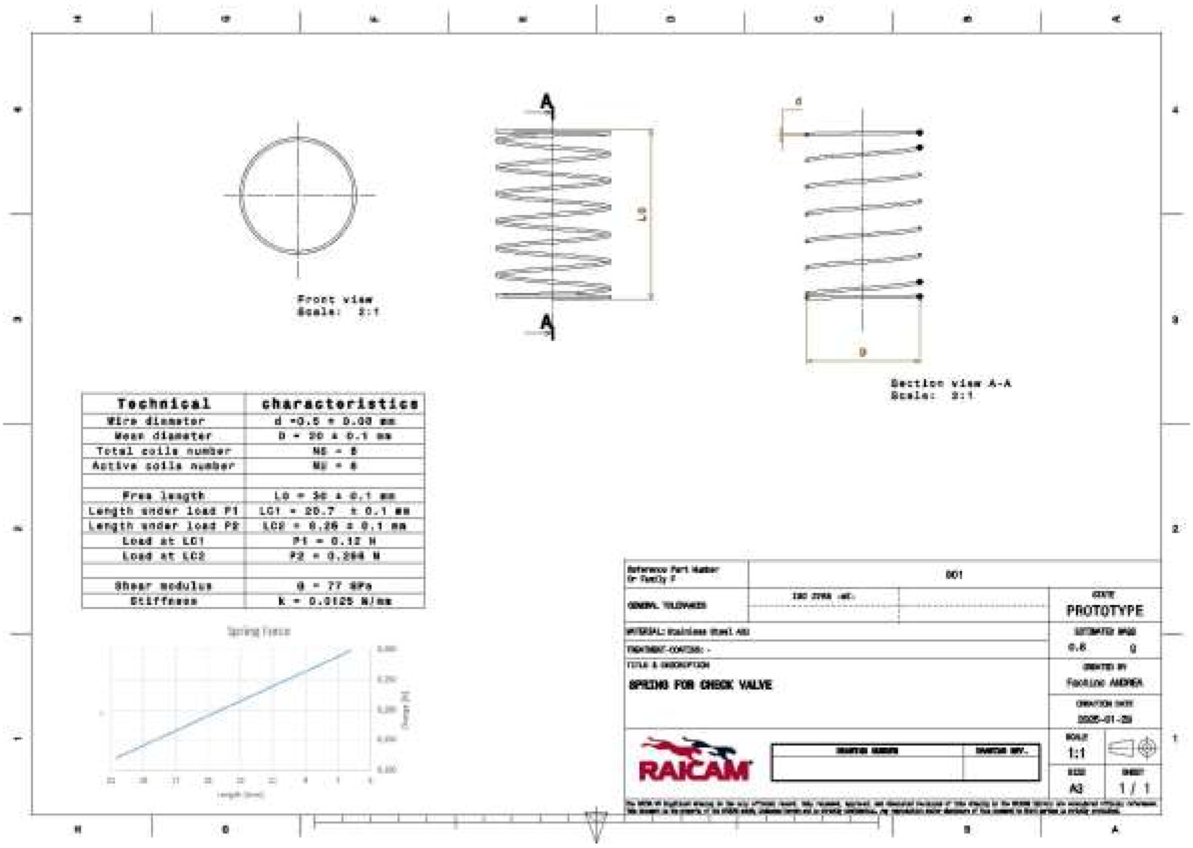

Figure A2.5: Spring for check valve_ technical drawing

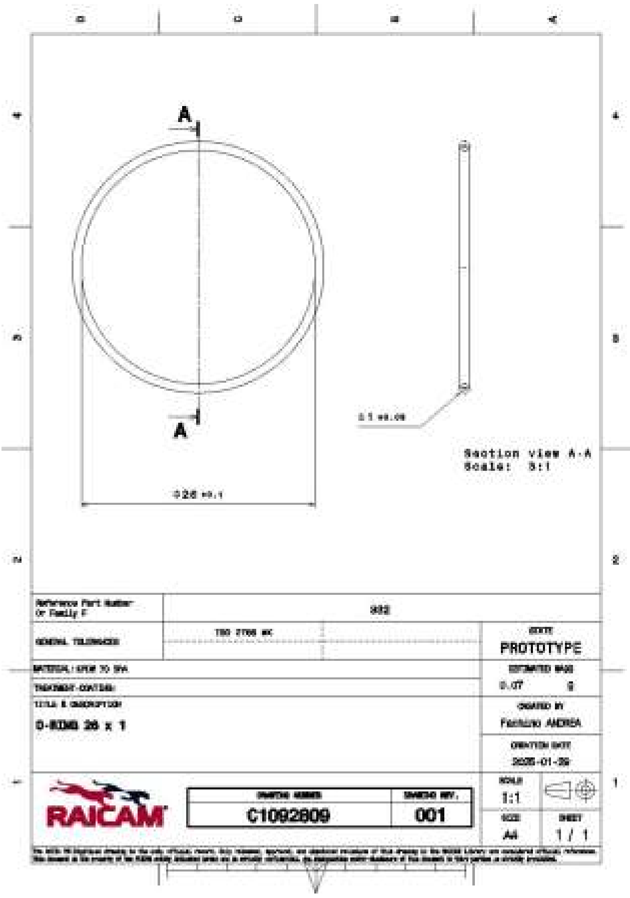

Figure A2.6: O-ring_ technical drawing

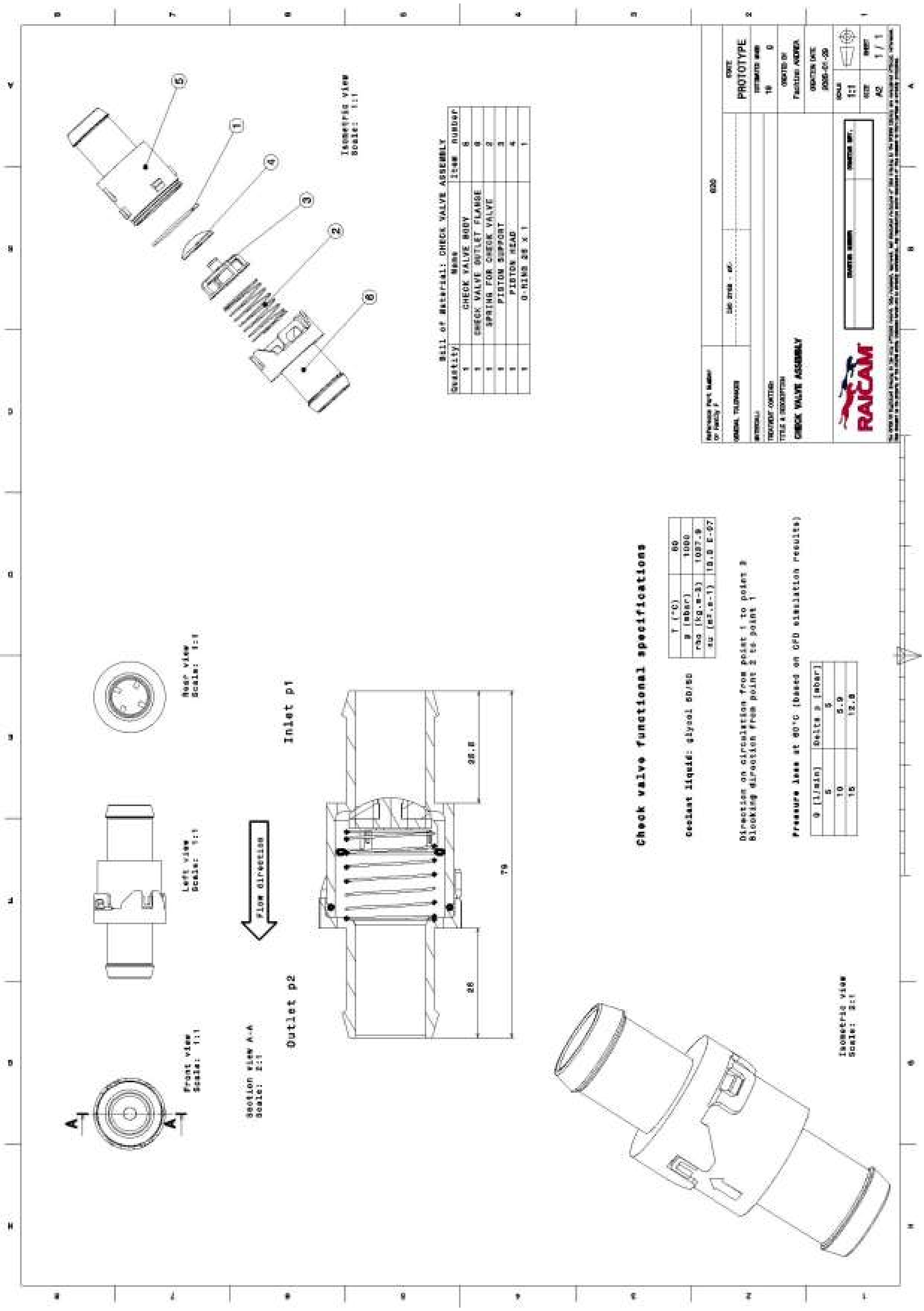

Figure A2.7: Check valve assembly_ technical drawing

Bibliography

[1] Raicam. [Online]. Available: https://raicam.com/cooling-systems.

[2] s. a. i. m. Raicam:Basic product training. [Online].

[3] B. Nesbitt, «Handbook of Valves and Actuators: Valves Manual International,» 2007.

[4] «Pressure drop,» [Online]. Available: https://www.dft-valves.com/blog/what-is-cracking-pressure/.

[5] IntelliMESUR®, «Series F Test Frames + IntelliMESUR® Software User's Guide,» [Online].

[6] «Microstructure and Properties of Glass Fiber-Reinforced Polyamide/Nylon Microcellular Foamed Composites.,» 2020.

[7] «PA material properties,» [Online]. Available: https://www.matweb.com/search/DataSheet.

[8] «Rotary friction welding,» [Online]. Available: https://www.researchgate.net/figure/Rotary-friction-welding-process_fig1_351986961.

[9] «Ultrasonic welding,» [Online]. Available: https://www.sciencedirect.com/topics/engineering/ultrasonic-welding.

[10] B. m. science, «Snap-Fit Joints for Plastics - A Design Guide.».

[11] C. Multiphysics, «Introduction to COMSOL Multiphysics,» [Online]. Available: https://cdn.comsol.com/doc/6.2.0.415/IntroductionToCOMSOLMultiphysics.it_IT.pdf.

[12] «Bernoulli Principle,» [Online]. Available: https://www.khanacademy.org/science/physics/fluids/fluid-dynamics/a/what-is-bernoullis-equation.